TITLE

Cerebellar patients have intact feedback control that can be leveraged to improve reaching

AUTHORS

Amanda M. Zimmet[a,b]
amandazimmet@gmail.com
ORCID ID: 0000-0003-1457-3072

Amy J. Bastian[b,c*]
bastian@kennedykrieger.org
ORCID ID: 0000-0001-6079-0997

Noah J. Cowan[d*]
ncowan@jhu.edu
ORCID ID: 0000-0003-2502-3770

*these authors jointly supervised this work

AUTHOR AFFILIATIONS

a. Johns Hopkins University Department of Biomedical Engineering
School of Medicine
720 Rutland Avenue / Ross 720
Baltimore, MD 21205, USA

b. Kennedy Krieger Institute
707 N. Broadway St.
Baltimore, MD 21205, USA

c. Johns Hopkins University Department of Neuroscience
School of Medicine
1003 Wood Basic Science Building
725 N. Wolfe Street
Baltimore, MD 21205, USA

d. Johns Hopkins University Department of Mechanical Engineering
223 Latrobe Hall
3400 North Charles Street
Baltimore, MD 21218, USA

CORRESPONDING AUTHOR

Noah J. Cowan
ncowan@jhu.edu
410-516-5301

Laboratory for Computational Sensing and Robotics
121 Hackerman Hall
3400 N. Charles Street
Baltimore, MD 21218, USA

ABSTRACT

It is thought that the brain does not simply react to sensory feedback, but rather uses an internal model of the body to predict the consequences of motor commands before sensory feedback arrives. Time-delayed sensory feedback can then be used to correct for the unexpected—perturbations, motor noise, or a moving target. The cerebellum has been implicated in this predictive control process, as cerebellar damage leads to deficits in movement control (e.g. poor targeting, oscillation) that are reminiscent of a poorly tuned control system. Here we show that the feedback gain in patients with cerebellar ataxia matches that of healthy subjects, but that patients exhibit substantially more phase lag. This difference is captured by a computational model incorporating a Smith predictor in healthy subjects that is missing in patients, supporting the predictive role of the cerebellum in feedback control. Lastly, we improve cerebellar patients' movement control by altering (phase advancing) the visual feedback they receive from their own self movement in a simplified virtual reality setup.

INTRODUCTION

Humans normally rely on a balance of feedback and predictive control mechanisms to make smooth and accurate movements. Proprioceptive and visual feedback are necessary for determining body postures at the beginning and end of a movement and can be used to guide slow movements accurately. However, feedback is time delayed, and thus it never represents the current state of the body during movement. Because of this, it is thought that we depend on internal models of the body that are built based on prior experience. These models can be rapidly accessed and thus provide a fast internal prediction system to estimate how a movement will

unfold, enabling us to better understand where our limbs are at any given moment. This allows us to make fast and accurate movements despite long-latency feedback.

People with cerebellar damage show a characteristic pattern of incoordination during movement that is referred to as ataxia. When reaching, they make curved movements that miss intended targets and require multiple corrections. This pattern of over- and undershooting a target (dysmetria) and oscillatory corrections (intention tremor) are hallmarks of cerebellar ataxia. One hypothesis that might explain ataxia is that the predictive estimation and control provided by cerebellar circuits is dysfunctional or lost (Wolpert, Miall, and Kawato 1998; R. Chris Miall et al. 2007).

Normally, the estimation of limb state (i.e., position and velocity) benefits from integrating proprioceptive measurements with an internal predictive control model during a movement (Paillard and Brouchon 1974; Adamovich et al. 1998; Fuentes and Bastian 2010). However, patients with cerebellar damage do not seem to receive this benefit (N. H. Bhanpuri, Okamura, and Bastian 2013; Weeks, Therrien, and Bastian 2017). Worse, it is possible that their predictive model actually conveys incorrect state information during active movements, which could corrupt rather than enhance proprioceptive estimation of limb state. This difficulty of predicting the future state of limbs during active movement leads to movements that are poorly directed and scaled, requiring ongoing corrections to reach a goal location.

Patients with cerebellar ataxia may rely more heavily on visual feedback to correct dysmetric movements (Beppu, Nagaoka, and Tanaka 1987; Beppu, Suda, and Tanaka 1984; Day

et al. 1998). A drawback of visual feedback is that it is slower than proprioception; intention tremor in these patients' movements is thought to stem from dependence on time-delayed visual feedback to make corrections (Day et al. 1998). However, it is not known how well they incorporate this visual feedback into their movements. Is visual feedback control impaired? Or does the dysmetria stem solely from errors in predictive (i.e., feedforward) control (M. Manto, Godaux, and Jacquy 1994; Nasir H. Bhanpuri, Okamura, and Bastian 2014; M. A. Smith and Shadmehr 2005)? A gait study by Morton and Bastian suggested that cerebellar patients could use feedback information to make reactive corrections during split-belt treadmill walking in order to maintain stability, but lacked the ability to adapt their predictive motor patterns (Morton and Bastian 2006). Other studies have indirectly supported the notion that patients can incorporate some level of visual feedback control in reaching (M. Smith, Brandt, and Shadmehr 2000; Day et al. 1998).

In this study, we used behavioral experiments and computational modeling to test for any impairment in visual feedback control (correction based on measured error) and disambiguate it from previously described impairments in feedforward control (Broersen et al. 2016; Bares et al. 2007). Subjects performed a visuomotor task which required them to track an unpredictable target (Roth et al. 2011). This method allowed us to determine that cerebellar patients can integrate visual feedback control similarly to healthy, age-matched control subjects. We then hypothesized that we could exploit intact feedback control to reduce dysmetria by dynamically altering visual feedback closed-loop in a simplified virtual reality setting. Specifically, we provided an acceleration-dependent alteration to visual feedback of a hand cursor to compensate

67 for time delays and allow patients to use feedback more effectively. This real time controller
68 successfully reduced patients' dysmetria.

69 METHODS

70 EXPERIMENTAL MODEL AND SUBJECT DETAILS

71 A total of 17 patients with cerebellar deficits and 14 age-matched controls were tested in
72 one or more of the following experiments. Patients were excluded if they had any clinical or
73 MRI evidence of damage to extra-cerebellar brain structures, or clinical evidence of dementia,
74 aphasia, peripheral vestibular loss, or sensory neuropathy. The age-matched controls were
75 clinically screened for any neurological impairments. Experiments 1-2 tested 11 cerebellar
76 patients (7 male, 4 female) and 11 age-matched controls (4 male, 7 female). Patient and control
77 ages were within +/-3 years of age. The one exception is a pairing of a 78 year old patient with a
78 71 year old control. Experiment 3 tested 12 cerebellar patients (8 male, 4 female) and 12 age-
79 matched controls (3 male, 9 female), and all patient and control ages were within +/-3 years of
80 age. Subjects gave informed consent according to the Declaration of Helsinki. The experimental
81 protocols were approved by the Institutional Review Board at Johns Hopkins University School
82 of Medicine. Each subject used his or her dominant arm for all tasks. The only exception was
83 one unilaterally affected cerebellar patient who was instructed to use her affected, non-dominant,
84 hand. We quantified each subject's ataxia using the International Cooperative Ataxia Rating
85 Scale (ICARS) (Trouillas et al. 1997). The results of the ICARS as well as demographic
86 information for all patients are shown in Table 1.
87

EXPERIMENTAL APPARATUS AND TASK INSTRUCTIONS

For all experiments, subjects were seated in a KINARM exoskeleton robot (BKIN Technologies Ltd., Kingston, Ontario, Canada), shown in Figure 1A, which provided gravitational arm support while allowing movement in the horizontal plane. A black video screen occluded the subjects' view of their arm movements. The shoulder position was fixed at a 75 degree angle, as shown in Figure 1C. The wrist joint was also fixed; therefore, the elbow joint was the only freely mobile joint. Data were recorded at 1 kHz. The KINARM system exhibits a cursor delay. Using a high-speed camera, we measured this delay (0.048s) and took the delay into account in modeling the human control system.

A 1 cm diameter white dot (cursor) was projected onto the display to indicate the subject's index fingertip position. The display was calibrated so that the projected dot position aligned with the subject's fingertip position. Subjects performed three experiments: sum-of-sines task (Experiment 1), single-sines task (Experiment 2), and discrete reaches (Experiment 3).

For Experiments 1 and 2, subjects were instructed to try to keep the cursor in the center of the target, a 1.5 cm diameter green dot (Figure 1C). The target angle followed a pseudorandom sum-of-sines (Figure 1D) or single-sine pattern. Each trial was 100 seconds long. We tested three different Feedback Gain conditions in the sum-of-sines (Experiment 1) task: 1.35 (cursor moves 35% farther than hand), 0.65 (cursor motion is attenuated by 35%) and 1.0 (veridical feedback; Figure 1B). Subjects were not informed that there was a gain change.

For Experiment 3, the robot moved the arm to align the cursor with the red dot start position (55 degree elbow angle) before each reach. After approximately 2 seconds, the red dot disappeared, and a green target dot (1.5 cm diameter, at 85 degree elbow angle) appeared elsewhere on the screen. Subjects were instructed to bring the white cursor dot to the center of the green target dot (a 30 degree flexion movement) as smoothly and accurately as possible without over or undershooting the target. If the fingertip did not reach within 1.75 of the target within 800 ms, the green dot changed to blue and subjects were instructed to complete the reach (trials were not repeated); the subjects were also asked to try to move faster on the next trial. The next trial started after the subject kept the fingertip in the target dot for two continuous seconds.

Healthy control subjects performed five practice trials and patients performed 10 practice trials to familiarize themselves with the procedure. If subjects were still confused about the procedure after the practice trials, they were given more practice trials until they were comfortable with the procedure.

Control subjects performed blocks of five reaches of each of the following Acceleration-Dependent Feedback Gain conditions, where the cursor angle was set to follow the elbow angle plus an acceleration-dependent term:

$$\text{CursorAngle(t)} = \text{ElbowAngle(t)} + k_a \frac{d^2}{dt^2}\text{ElbowAngle(t)}$$

The 8 gain conditions tested were k_a = 0, 0.005, 0.010, 0.015, 0.020, −0.005, −0.010, −0.015, and −0.020. Subjects were given five trials of one Feedback Gain before being exposed to the next Feedback Gain on the list. This was to encourage subjects to focus on the white dot

position. Trial order was not randomized because in pilot experiments, when the gains were randomized, the subjects seemed to focus on their proprioception rather than the visual feedback.

Cerebellar patients performed blocks of 10 reaches with a single Acceleration-Dependent Feedback Gain. Patients started with an Acceleration-Dependent Feedback Gain of 0 (veridical feedback). Individual reaches were categorized as hypometric, on-target, or hypermetric. Based on the mode of this categorization for the 10 reaches, the Acceleration-Dependent Feedback Gain was increased, remained the same, or decreased. The amount by which the Acceleration-Dependent Feedback Gain was altered was determined using the Parameter Estimation by Sequential Testing (PEST) algorithm (see Implementation of the PEST Algorithm (Experiment 3)) (Taylor and Creelman 1967). We also tested six of the twelve cerebellar patients on the control subject task (blocks of 5 trials on the 8 gains listed above); others could not due to time constraints.

Some subjects completed only a subset of the experiments due to time constraints. For every experiment, between trials, subjects were told to relax while the robot moved the subject's hand to bring the cursor to the start position.

EXPERIMENTAL DESIGN AND STATISTICAL ANALYSIS

Generating the Sum-of-Sines Target Trajectory (Experiment 1)

The goal of Experiment 1 was to determine how well patients and controls could track an unpredictable sum-of-sines stimulus and probe their ability to use visual feedback for movement control. The target trajectory comprised 15 sine waves whose frequencies were prime multiples

of 0.05 Hz, namely 0.1, 0.15, 0.25, 0.35, 0.55, 0.65, 0.85, 0.95, 1.15, 1.45, 1.55, 1.85, 2.05, 2.15, and 2.35 Hz. Phases of each sinusoid were randomized. Each trial was 100 s long, comprising five replicates of the sum-of-sines trajectory. The sinusoids were scaled so that the *angular velocity* of each sinusoid never exceeded 720 degrees per second while the *positional* amplitude of each sine wave never exceeded 2 degrees. The non-harmonic relation of the component sinusoids created a temporally complex target motion with 45 degrees of freedom (amplitude, phase, and frequency for 15 sinusoids) that repeats every 20 s; a portion of the trajectory is shown in Figure 1D, wherein it can be observed that the signal trajectory includes multiple seemingly random turn-arounds within even very short timescales. This complexity, coupled with the long period, makes this target motion far less predictable than a simple single-sine motion (Roth et al. 2011). Lastly, the dramatic increase in tracking phase lag presented in this paper (see Results) for sum-of-sine responses recapitulates the main finding of (Roth et al. 2011), confirming that from a practical point of view subjects were less able to predict the movement trajectories. Nevertheless, this signal design allowed good signal-to-noise ratio at each frequency while avoiding excessively large or fast motions of the target, making it well suited as a probe signal for tracking behavior (Roth et al. 2011). The normalized magnitude of Fourier spectrum of our input signal is shown in the top half of in Figure 1E. Five trials were conducted for each condition tested.

Estimating Frequency Response from the Sum-of-Sines Data (Experiment 1)

All analysis was performed using custom scripts in MATLAB (The Mathworks Inc., Natick, MA, USA). To obtain the steady-state frequency response of the subject, the first period (20 seconds) was discarded as transient, leaving four periods per trial. The data were manually

inspected for unusual activities that were not representative of the subject's typical behavior. For example, if the subject turned away from the screen to cough or talk, movement would cease for a few seconds and the data from those few seconds were removed from further analysis. The movement trajectories for a given subject were then averaged across trials at each time instant, excluding any deleted data. The averaged data were linearly detrended and converted to the frequency domain via the discrete Fourier transform (DFT). An example of the result of this process for a cerebellar patient is shown in Figure 1F (the frequency domain data is complex valued at each frequency so only the magnitude is shown). To estimate a subject's frequency response, we calculated the ratio of the DFT of the subject's movement to the DFT of the underlying target trajectory at each of the 15 frequencies in the sum-of-sines. The result of this calculation is 15 complex numbers, called *phasors*, representing the frequency response estimate for a given subject. The magnitude of each phasor is the *gain* and the angle is the *phase* of the subject's response at that frequency.

Phasor Plot

To visualize the frequency response, we used Phasor Plots as shown in Figure 2A. In these plots, the gain is the radial distance from the origin, and phase lag is the clockwise angle of the data with respect to the horizontal axis. Perfect tracking at a given frequency corresponds to unity gain and zero phase lag, as illustrated by the large blue dot in Figure 2B. The distance between any point on the phasor plot and this blue dot provides a measure of the amplitude of the (sinusoidal) error signal at that particular frequency as a proportion of the input signal amplitude.

Additionally, this visualization can be enhanced with a circle with a 0.5 radius centered at +0.5 along the horizontal axis as shown in blue in Figure 2B. Points on this circle correspond to the ideal response gain for minimizing error given a particular phase lag (Roth et al. 2011). Points on this circle represent the gain values that minimize error assuming the subject cannot further minimize phase lag. Points outside the circle indicate the subject is moving too much for a given phase lag, i.e., if they moved with a lower amplitude they would achieve a lower tracking error. Points within the circle may represent striking a balance between effort and error in that the subject is not moving enough to fully minimize their error given a certain phase lag. Lastly, points that lie on the unit circle, traced in bold black in Figure 2C, would indicate that the subject is replicating the sinusoidal component exactly, albeit at a phase shift.

Phasor Plot Scaling

If a subject were to "fully" respond to an applied visual gain, the subject would need to scale his or her movement so that the visual output appeared the same as it did in the veridical feedback condition, although there is no constraint (or instruction) to do so. In reality a subject may scale his or her movements more than this, less than this, or even not at all. To quantify this, we fit a Scaling Factor that, when multiplied by the frequency response phasors for a given Feedback Gain condition, best aligned the phasors with those of the veridical condition. We only included the five lowest frequencies in this calculation because at these frequencies subjects generally appeared to have robust responses (based on visual inspection of the data). At high frequencies, however, response magnitudes were low and therefore fitting the Scaling Factor could be dominated by noise.

Scaling Factor (dependent measure) was analyzed using a 2-way ANOVA, testing for the effects of two independent variables, group (patient vs. control) and Feedback Gain (0.65 and 1.35). If a main effect was found to be significant, we calculated an effect measure (η_p^2) using the Measures of Effect Size toolbox for Matlab (Hentschke and Stüttgen 2011).

Model Fitting and Model Selection

To capture the visuomotor tracking response of both cerebellar patients and age-matched healthy controls, we adapted the classic McRuer gain-crossover model: a delayed, scaled integrator which specifically assumes that the subject is responding to an unpredictable stimulus (McRuer and Krendel 1974). We hypothesized that the patient and control models would be equivalent except for the magnitude of the feedback delay. To test this, we considered a more general class of models that allows for distinct parameters for the healthy subjects and controls, and includes the possibility of distinct delays on the visual measurement of target motion from that of self-movement feedback (which can incorporate for example, proprioception, which generally incurs a lower latency than visual). To determine the simplest combined model of patients and controls which provided both a good and consistent fit without overfitting, we used a model selection process similar to that described in (Madhav et al. 2013) based on Experiment 1 data (sum-of-sines). In the most flexible model, all patient and control parameters were allowed to vary independently with eight free parameters: $k_{patient}$, $k_{control}$, Visual $Gain_{patient}$, Visual $Gain_{control}$, Visual $Delay_{patient}$, Visual $Delay_{control}$, Feedback $Delay_{patient}$, and Feedback $Delay_{control}$. The following model selection procedure aimed to determine which of those eight parameters should be free and which should be yoked together. Different combinations of yoked parameters

were tested as well as different model structures. Some of these model structures allowed for the elimination of one or more of the blocks within the model structure.

The following procedure was repeated for each possible model. For each subject, we represented their frequency response as an array of 15 complex numbers (one for each of the frequencies tested in the sum-of-sines experiment). We began by pulling 10 of the 11 age-matched patient–control pairs from the full dataset. Then, we took the average of those 10 patients' (and, separately, controls) frequency responses at each tested frequency. Using the MATLAB function 'fminsearch,' we used these average frequency response functions to fit the current model parameters to the average data by minimizing the frequency-domain (FD) error:

$$\text{FD-error} = \|\text{control}_{\text{left out}} - \text{control}_{\text{model fit}}\|^2 + \|\text{patient}_{\text{left out}} - \text{patient}_{\text{model fit}}\|^2 \quad (1)$$

where *control* and *patient* in the above equation were arrays with 15 complex values, corresponding respectively to frequency responses of healthy control subjects and patients at the 15 frequencies tested. This was repeated 100 times with different initial parameter values selected for the 'fminsearch' function, increasing the likelihood of finding a global minimum. The model parameters that generated the lowest overall error were kept (as well as the magnitude of the error). This was repeated for each patient–control pair, yielding 11 sets of model parameters and 11 leave one out error values.

The leave one out error values were averaged together to create the gross leave one out error for that model structure. This was our gauge for the ability of the model to capture the responses. The maximum singular value of all 11 sets of the model parameters for that particular

model was used as our gauge for model consistency. This was repeated for all potential models. We then selected a best model based on the tradeoff of model fit, model consistency, and number of free parameters. Finally, we used bootstrapping to generate confidence intervals for the parameter values in our best model.

We validated the frequency-domain fits in the time domain. We converted each frequency-domain model (which includes patient and control submodels) to state space in Matlab, and simulated the model pair using the lsim command (Figure 4S2). The input was the sum-of-sines target angle trajectory used in experiments. The model output produced a distinct prediction for the elbow-angle trajectory for each group (patients and controls; Figure 4C). These simulated elbow-angle responses were compared to subject responses as follows. We averaged across trials for each subject to compute a single time-domain response for each patient and each age-matched control; we then averaged across subjects in each group to compute a mean elbow-angle response for patients and a mean elbow-angle response for controls. Given the simulated model responses and actual patient and control mean responses, the time-domain (TD) error was calculated as follows:

$$\text{TD-error} = \int_{20}^{100} (\text{control}(t)_{\text{mean}} - \text{control}(t)_{\text{model}})^2 + (\text{patient}(t)_{\text{mean}} - \text{patient}(t)_{\text{model}})^2 dt$$

where the integration is taken over the last 80 seconds of the 100s trial period. The TD-error was normalized so that the maximum error was 1 for visualization purposes.

Generating the Single-Sines Trajectory (Experiment 2)

In Experiment 2, we wanted to determine how well patients and controls could track a predictable single sine wave. Every other frequency tested in the sum-of-sines condition was tested as a single, standalone sine wave: 0.1, 0.25, 0.55, 0.85, 1.15, 1.55, 2.05, and 2.35 Hz. The amplitude of each sine wave matched (component-wise) the sum-of-sines experiments. Subjects

were once again instructed to keep the cursor in the target dot as much as possible. The order of presentation of the stimuli was randomized for each subject.

Processing the Single-Sines Data (Experiment 2)

The processing of the data for the single-sine condition was identical to the processing of the sum-of-sines data, except that there was no averaging across trials and no manual inspection/filtering of the data for unusual activities. This is because we were only looking at one frequency from each sine wave trial, and any error caused by an unusual, aperiodic activity (such as pausing) would introduce very little power at any individual frequency.

Comparing Phase Lags between Sum-of-Sines and Single-Sine Conditions (Experiments 1 & 2)

We tested whether the cerebellar group showed a different pattern of phase lag across frequencies compared to controls. Specifically, we compared the phase lag for the lowest common frequencies (0.10, 0.25, 0.55, 0.85, 1.15) in the sum-of-sines and single-sine conditions across the two groups. We hypothesized that the control group would be able to use prediction and follow the single sine wave with little phase lag compared to the cerebellar patients. We expected that there would be less of a difference between groups when they followed the sum-of-sines. We used a parametric two-way ANOVA for circular data called the Harrison-Kanji test for this analysis (Berens 2009).

Implementation of the Acceleration-Dependent Feedback Gain for Experiment 3

In Experiment 3 we attempted to improve dysmetria for discrete reaching by individually optimizing visual feedback gains. Using the KINARM's real-time computer, we calculated the average of the previous 100 elbow angular acceleration values (at 1 kHz sampling, this resulted in a ~ 50 ms delay) as an approximation of the instantaneous acceleration. This instantaneous acceleration was multiplied by the Acceleration-Dependent Feedback Gain (k_a), added to the real elbow angle, and the position of the cursor was displayed on the Kinarm screen at this new, slightly shifted angle.

Quantification of Dysmetria for Experiment 3

We quantified dysmetria in this single-joint task by measuring the elbow angle at which the subject made his or her first correction. In a smooth and accurate reach, the ratio between the angle of first correction and the goal angle would be 1. We determined the angle of the first correction by finding when the velocity crossed zero after the initiation of the reach. The angle of the elbow at this time point is the angle of the first correction. This angle was divided by the goal angle of 30 degrees. If the result was greater than 1.03, the reach was categorized as hypermetric, and likewise, if the result was less than 0.97, the reach would be categorized as hypometric. Results between 0.97 and 1.03 were classified as "on target" reaches.

Implementation of the PEST Algorithm (Experiment 3)

The Parameter Estimation by Sequential Testing (PEST) algorithm was used to iteratively determine the best Acceleration-Dependent Feedback Gain values to apply in Experiment 3 by analyzing the history of the responses to different applied values (Taylor and

Creelman 1967). If the mode of the initial set of reaches was hypermetric, the Acceleration-Dependent Feedback Gain would be decreased. Likewise, it would be increased if the mode of the set was hypometric. The initial step size used for the PEST algorithm was 0.01. The maximum step size for the PEST algorithm was limited to 0.01 and the minimum step size was 0.0035. The maximum Acceleration-Dependent Feedback Gain was set to +/-0.02. The PEST algorithm was terminated when two blocks of the same Acceleration-Dependent Feedback Gain yielded a mode of reaches classified as "on target." Alternatively, if this portion of the experiment took longer than approximately 20 minutes or the subject was experiencing fatigue, the most successful Acceleration-Dependent Feedback Gain was selected based on those which had already been tested. To show the effects of the full spectrum of Acceleration-Dependent Feedback Gains on cerebellar patients, we also had 7 cerebellar patients complete the control task in addition to the PEST block.

RESULTS

Experiment 1: Cerebellar Patients and Age-Matched Controls Respond Similarly to Rescaling of Visual Self-Motion Feedback

To probe participants' ability to use visual feedback, we challenged cerebellar patients and age-matched controls to keep a cursor within a target dot that was following an unpredictable trajectory. The normalized Fourier spectrum (magnitude only) of the target trajectory is shown in Figure 1E and the spectrum of a single subject's response is shown in Figure 1F. Note that this subject had clear peaks at all of the frequencies of target movement in the veridical condition (1x).

Subjects also were exposed to two Feedback Gain conditions where the cursor was presented at 0.65x or 1.35x. A phasor plot for each Feedback Gain condition is shown for a single cerebellar patient in Figure 3A. Points with the smallest phase lag (~30°) are responses from the lowest frequencies (0.1 Hz). Responses at the five lowest frequencies are marked with solid dots. As the input frequency increases, the phase lag increases and the plotted points move progressively clockwise around the origin. At the lowest frequencies, note from Figure 3A that the subject scales his movement in response to the Feedback Gain applied. For the 0.65 Feedback Gain condition, he increases the scaling of his movement in comparison to the veridical condition, as expected. Similarly, in the 1.35 Feedback Gain condition, he decreases the scaling of his movement in comparison to the veridical condition.

For each patient, we computed a Scaling Factor based that best scaled responses at the lowest 5 frequencies (Methods); to visualize how well this Scaling Factor represents our data, the Response Gain data from the cerebellar patient in the 1.35 Feedback Gain condition shown in Figure 3A is multiplied by its scaling factor to yield the corresponding line in Figure 3B. If the scaling factor is a good fit for the data, the data should rest on top of the veridical line. Note that the phase is not modified by this scaling computation, so we should not expect to see an improvement in phase alignment in this second plot.

Figure 3C shows the Scaling Factors for all subjects for each Feedback Gain condition. We conducted a one-sided t-test to determine whether patients scaled their gain in the hypothesized direction against the null hypothesis that patients' scaling factors would be 1 (i.e.,

381 they would not respond to the applied feedback gain). Both groups scaled up (patients: $p<0.05$,
382 $t=-2.1$, DOF=10; controls: $p<5x10^{-6}$, $t=-8.3$, DOF=10) or scaled down (patients: $p<0.005$, $t=3.23$,
383 DOF=10; controls $p<0.0005$, $t=5.3$, DOF=10) their movement, commensurate with the
384 respective decrease or increase of the cursor Feedback Gain. We performed a two-way ANOVA,
385 confirming that the effect of Feedback Gain (0.65 vs. 1.35) on Scaling Factor was highly
386 significant ($F(1,40)=59.7$, $p<2x10^{-9}$, $\eta_p^2=0.7$), whereas the effect of group (patient vs. control) on
387 Scaling Factor was not significant ($F(1,40)=0.05$, $p=0.83$), with no significant interaction
388 between group and gain ($F(1,40)=3.57$, $p=0.07$). We accounted for the samples being dependent
389 on one another because each subject was exposed to both the 0.65 and 1.35 gain conditions. The
390 effect size was computed using the Hentschke and Stüttgen toolbox (Hentschke and Stüttgen
391 2011).
392
393 Note that the Scaling Factor in for the gain of 1.35 was typically approximately 1.2.
394 Intuitively, this indicates that subjects rescaled their movements as if to compensate perfectly for
395 an experimentally applied Feedback Gain of 1.2, i.e., they did not fully compensate for the
396 change in gain. Likewise, for a Feedback Gain of 0.65, the Scaling Factor was typically
397 approximately 0.8, again implying that subjects compensated, albeit not fully, for the visual
398 rescaling (Figure 3). Critically, the patients' responses to the feedback scaling were comparable
399 to that of age-matched controls, suggesting that they were able to use visual feedback in a
400 substantively similar manner.
401

402 ## Cerebellar Patient Performance Best Captured by Long Latency Closed-Loop Model

403 In computational terms, one can interpret the data from Experiment 1 to mean that
404 cerebellar patients had a functional feedback loop in their control system. Here we asked if they
405 are using the same "control structure" (i.e., a model of the interplay between sensory feedback,
406 external sensory input, and motor output) as age-matched controls. Because the cerebellar and
407 age-matched control groups scaled their movements similarly in Experiment 1, one might
408 hypothesize that they were using a similar control structure. However, the scaling was measured
409 relative to each subject's baseline movement in the veridical condition and was not a measure of
410 their overall error performance on the task; for example, issues of phase lag would not be
411 captured by the scaling analysis. Thus, here we use our findings from Experiment 1 along with
412 the model selection procedure described by Madhav et al. (2013) to determine any differences in
413 control structures used by patients and age-matched controls.
414
415 Consider the hypothesized model depicted in Figure 4A. In this model, the brain
416 calculates the error between perceived elbow angle and target angle, as shown in the subtraction
417 calculation in the feedback diagram. The model merges the cascade of the subject's internal
418 controller and mechanical plant (arm and robot dynamics); the combined plant and controller is
419 treated as a classic McRuer gain-crossover model—a scaled integrator—a model based on the
420 assumption that the subject is responding to an unpredictable stimulus (McRuer and Krendel
421 1974). Our hypothesis is that all model parameters would be equivalent between patients and
422 age-matched controls, except that patients would have a feedback delay commensurate with their
423 visual processing time (~140-250 ms) and controls would have a lower-latency feedback delay
424 commensurate with their proprioceptive feedback processing time (~110-150 ms) (Cameron, de

425 la Malla, and López-Moliner 2014; N. H. Bhanpuri, Okamura, and Bastian 2013). This is
426 because we expect that patients would rely more on (slower) visual feedback to compensate for
427 their deficient estimation of limb state.
428
429 To test this hypothesized model, we performed model fitting and model selection based
430 on 60 related models (Figure 4S1A,B). Our hypothesized model was just one possibility and the
431 parameter values of the models were not constrained *a priori*. The models were compared based
432 on joint consideration of model consistency and model fit. Model fitting and selection produced
433 four models (called Models W, X, Y, and Z) that were nearly equivalent in their trade-off
434 between model inconsistency and model fitting error (Figure 4S1C). Moreover, three of the four
435 models (Models X, Y, and Z) were extremely similar in their structure and parameters (Figure
436 4S1D and Table 2). One of these, Model Y, matched our hypothesis (Figure 4A) except that
437 feedback delay from control subjects was shorter than we hypothesized (30ms, see Table 2).
438 Model W differs slightly in model structure and parameters but also exhibits a smaller feedback
439 delay for controls than patients. Indeed, in all four top models, the feedback delay was
440 substantially shorter for control subjects than cerebellar patients. This suggests that controls can
441 rely on an internal model of their hand position and/or proprioceptive feedback to make
442 corrections for their future movements while cerebellar patients must rely on delayed visual
443 feedback (see Discussion). We selected Model Z as the Best Model on the basis of it having the
444 fewest free parameters of the top four models (*Figure 4*B). This Best Model closely matches our
445 hypothesis except that it does not include any feedback delay for control subjects.
446

In addition to the parameter values having consistent values across the top four models, they also have intuitively plausible values (*Table 2*). While the true parameters have biological limitations, we did not restrict their values during the fitting procedure. This provides a useful diagnostic tool, since unrealistic parameter fits would indicate inadequate model structure. In three of the models (Models X, Y, and Z) Visual Delays were found to be 170 ms, which is biologically plausible. The tight consistency of visual delay is likely a reflection of the fact that model fitting accuracy is expected to be quite sensitive to phase differences, and in our model, delay has the biggest impact on phase, so that parameter is expected to be highly constrained by the data. Model W exhibited a low Visual Delay of 110ms for controls, equal to the feedback delay for controls. One possible explanation for this model is that the sum-of-sines trajectory was not completely unpredictable and subjects were able to reduce feedforward latency with partial anticipation. Visual Gain values were all approximately 0.40 which also seems reasonable given a visual inspection of the data: subjects do not appear to be attempting to replicate the full magnitude of the signal, but some smaller portion of the signal.

As a final test of our modeling approach, we examined how our Best Model's (Model Z) parameters changed when we applied variations in Feedback Gain as shown in Table 3. Recall that in the 1.35 Feedback Gain condition, the dot moves more than the person's hand position; therefore, we expect the subject to move slightly less than they do in the veridical feedback condition because they do not need to move as much to get the same visual output (i.e., we expect k to decrease). Similarly, we expect the subject to attempt to replicate a greater portion of the signal because it is easier to do so. Thus, we expect the Visual Gain (the amount of the input signal that the subject is trying to reproduce) to increase with respect to the veridical condition.

Recall that the Visual Gain affects the *input* to the visual error computation. We expect the opposite trend for the 0.65 Feedback Gain condition, as is detailed in Table 3. Given that we believe the delays are biologically limited based on transmission time of visual information, we expect the delay magnitudes to stay the same between Feedback Gain conditions. Indeed, the model parameters change in the hypothesized manner when different Feedback Gains were applied. The results from fitting the Best Model to the data from each of the different Feedback Gains yields the parameter values shown in Table 4. The visual feedback delays are nearly identical between Feedback Gain conditions, and the k and Visual Gain values increase and decrease as hypothesized in Table 3. The one difference between the hypothesis and these model values is in the lack of a feedback delay for the control subjects. This discrepancy is addressed in the Discussion section.

Lastly, we used bootstrapping to generate confidence intervals for the parameter values in our Best Model. Making one change to the fitting procedure described earlier, after the leave-one-out step, we randomly sampled ten times with replacement from the remaining ten subjects. This was repeated 1000 times to generate 1000 sets of parameter values. From these values, we found the 95% confidence intervals for our best model to be: 2.4-2.7 for $k_{patient}$ and $k_{control}$; 0.38 - 0.41 for Visual $Gain_{patient}$ and Visual $Gain_{control}$; and 0.16-0.18 for Visual $Delay_{patient}$, Visual $Delay_{control}$, and Feedback $Delay_{patient}$.

490 ## Experiment 2: Poor Tracking of Simple Oscillatory Trajectories Highlights Cerebellar
491 Patients' Predictive Deficit

492 We validated the sinusoidal tracking paradigm by quantifying a known behavioral deficit
493 in cerebellar visuomotor control. In this predictable task, we expected healthy participants would
494 be efficient, exerting less than or equal to the amount of effort required to minimize error for a
495 given phase lag. Where subjects lie relative to this tradeoff can be visualized on a phasor plot;
496 efficient tracking would yield points on or inside the effort/error tradeoff circle (Figure 2B,
497 Methods). We hypothesized that patients with impaired prediction may in some cases exert more
498 effort than needed to minimize error, resulting in phasor points outside the effort/error tradeoff
499 circle. We also hypothesized that patients would generate larger tracking errors.
500

501 At the five lowest frequencies tested, all of the control responses landed in/on the circle,
502 whereas only 31% of patient responses landed in/on the circle (Figure 5). Additionally, patients
503 generated larger tracking errors: 70% of patient responses exhibited larger error magnitude than
504 the respective age-matched control responses. Furthermore, we created an aggregate tracking
505 error for the single-sines experiment by calculating the sum of the tracking errors for the lowest
506 five frequencies. We compared the aggregate tracking error between patients and age-matched
507 controls by calculating the difference for each pair and testing those differences against 0 using a
508 two-sided sign test. The null hypothesis for a two-sided sign test is that there was no difference
509 between patients and their age-matched controls. The alternative hypothesis is that the controls
510 may be either better or worse than patients. When we compared the difference between the
511 aggregate tracking errors for each patient/control pair to 0, controls were significantly better than
512 patients at single-sines tracking with 10 out of 11 controls performing better than their age-

513 matched counterpart ($p<0.05$). These results illustrate cerebellar patients' poor predictive ability.
514 Importantly, note that this analysis does not distinguish what portion of their errors stemmed
515 from poor prediction of the stimulus trajectory versus poor control of the arm.
516
517 For comparison, we also included the results from the task where the stimulus was
518 unpredictable (sum-of-sines from Experiment 1) in Figure 5. For this experiment, we expected
519 that patients would be less impaired relative to controls because neither group would be able to
520 predict the target trajectory. Indeed, patient and control behaviors were more similar in this
521 condition: for the five lowest frequencies tested in the sum-of-sines condition, 72% of control
522 responses and 64% of patient responses were in/on the circle. Note, however, that there is an
523 increased phase lag of the cerebellar patients (relative to controls), particularly as the frequency
524 of the stimulus increases, which would be expected if the patients were dependent primarily on
525 time-delayed visual feedback (feedback delay introduces greater phase lag at higher frequencies).
526 Specifically, 73% of individual patient frequency responses were more phase lagged than the
527 responses of the age-matched control (as computed on an individual frequency basis).
528
529 As expected, we also observed a reduction in tracking error from the sum-of-sines task to
530 the single-sines task. We calculated the magnitude of the tracking error for each subject for each
531 frequency (i.e., for the frequencies that were tested in both conditions) and then compared the
532 errors between the conditions. 93% of controls' and only 75% of patients' tracking errors were
533 reduced in the single-sine task in comparison to his or her performance in the sum-of-sines task.
534 Again, we computed the aggregate tracking error for the sum-of-sines task, as described earlier,
535 using the same five frequencies used in the single-sines aggregate tracking error calculation. We

536 then used a two-sided sign test to determine that patients ($p<0.001$) and controls ($p<0.001$) were
537 better at tracking single-sines than sum-of-sines, with all patients and all controls having less
538 tracking error for single-sines than sum-of-sines.

539 To specifically look at phase lag between groups (cerebellar vs. controls) and conditions
540 (single- vs. sum-of-sines), we used a circular statistical approach. Figure 6 shows polar
541 representations of the phase lags from the single-sine and sum-of-sines conditions (Figures 6A,
542 C) and an example time series from a control and cerebellar subject tracking the 0.85 Hz sine
543 wave (Figures 6B, D). The example control subject showed little phase lag suggesting that this
544 individual could make use of an internal prediction of the dot movement and their arm
545 movement. In contrast, the example cerebellar subject showed a systematic phase lag suggesting
546 that their ability to use prediction is impaired. The pattern of lag can be visualized across
547 frequencies in the polar plots. As a group, controls show a small increase in lag as the frequency
548 increases in the single-sine condition, whereas the cerebellar group shows large lags (Figures 6A
549 and C, compare purple vectors). Circular ANOVA for the single-sine condition showed that the
550 cerebellar group had greater lags compared to controls (Group effect, $p<0.001$), that the lags
551 increased with frequency (Frequency effect, $p<0.001$) and an interaction such that the cerebellar
552 group lags increased more than controls across frequency (Interaction effect, $p<0.001$). In the
553 sum-of-sines condition, the difference in lags across frequency was qualitatively less when
554 comparing cerebellar and control groups (Figures 6A and C, compare black vectors). Overall the
555 cerebellar group showed greater phase lags compared to controls (Group effect, $p<0.001$), but
556 there was a statistically borderline effect of Frequency (Frequency effect, $p=0.02$), and Group x
557 Frequency interaction (Interaction effect, $p=0.03$), which was weaker than that seen in the single-
558 sine condition.

Experiment 3: Virtual Reality Feedback Visual Feedback Reduces Dysmetria

The results from Experiment 1 indicated that cerebellar patients' feedback control may be intact. In Experiment 3, we leveraged this intact element of their control system to reduce dysmetria. Our goal was to provide each cerebellar patient with customized visual position feedback information that took into account their controller's mismatched feedforward model. This altered visual feedback would help them generate the correct motor command for a simple elbow movement (30 degrees flexion) by accounting for their actual arm dynamics.

Here we used a motor task that requires subjects make a discrete movement to a target that is stepped to a new position. This was chosen so that we could compare our data to previously published results using the same task with cerebellar patients. Subjects were asked to make a 30 degree elbow flexion movement from a home target to a stepped target. The task was completed with both veridical visual feedback and with altered visual feedback that was designed to reduce their dysmetria.

Bhanpuri et al. theorized that cerebellar patients have a static mismatch between their controller's internal model of their limb inertia and the actual limb inertia for elbow flexion movements (Nasir H. Bhanpuri, Okamura, and Bastian 2014). Critically, for single-joint elbow flexion or extension, an inertial mismatch causes an acceleration-dependent error in the internal dynamic model because inertia and acceleration are kinematically yoked. Thus, we predicted that an Acceleration-Dependent Feedback Gain (block diagram inset in Figure 7A) could provide corrective feedback to enhance reaching performance of cerebellar patients. Specifically, we took a subject's estimated acceleration (see Methods), multiplied this by the Feedback Gain, and

582 then added it to the position of the subject's cursor. We predicted that positive Acceleration-
583 Dependent Feedback Gains would make a subject more hypermetric and negative Acceleration-
584 Dependent Feedback Gains would make a subject more hypometric. Thus, we expected
585 hypometric patients would experience a reduction in dysmetria with a positive Acceleration-
586 Dependent Feedback Gain. Similarly, we expected hypermetric patients would experience a
587 reduction in dysmetria when a negative Acceleration-Dependent Feedback Gain was applied.
588
589 Subjects completed 30 degree elbow flexion reaching movements in the Kinarm
590 exoskeleton robot. Reaches were categorized as hypometric, hypermetric, or on-target based on
591 the angle where they made their first correction to their movement. Acceleration-Dependent
592 Feedback Gains were applied to the visual feedback provided on the Kinarm screen. For more
593 details on the implementation and instructions of this task, see Methods.
594
595 When an appropriate Acceleration-Dependent Feedback Gain was applied, dysmetria was
596 reduced. The effect of this Acceleration-Dependent Feedback Gain on the displayed trajectory is
597 shown in Figure 7A, where the dashed green line shows the altered visual feedback given to the
598 subject and the solid green line shows the subject's actual reach to the target for a single
599 Feedback Gain condition. Increasing the Acceleration-Dependent Feedback Gain magnitude had
600 a graded effect on the trajectory profile, as shown by the decreasing amplitude of the solid traces
601 in Figure 7A. Applying this Acceleration-Dependent Feedback Gain shifted the angle of first
602 correction in the way we predicted, as shown in both Figure 7B and C (control subjects also
603 respond similarly, Figure 8). Namely, positive Acceleration-Dependent Feedback Gain made
604 patients more hypermetric and negative Acceleration-Dependent Feedback Gain made patients

605 more hypometric. Thus, subject-specific Acceleration-Dependent Feedback Gain was needed to
606 best reduce dysmetria. In general, increased Acceleration-Dependent Feedback Gain magnitude
607 was needed to ameliorate greater dysmetria.
608

609 DISCUSSION

610 We found that cerebellar patients can use visual feedback control in a manner similar to
611 control subjects. This was assessed during a sum-of-sines visuomotor tracking task by subtly
612 changing the gain of the visual cursor feedback (i.e. hand) and measuring the degree to which an
613 individual subject could modulate the gain of his or her corrective movements. Our modeling
614 corroborated this finding: the structure and parameters differed between patients and controls
615 only in the feedback delay term. The patients relied on time delayed cursor feedback of their
616 hand position, whereas controls appeared to be able to generate predictions of their hand
617 position.

618 We also saw increases in phase lag for patients versus controls when following
619 predictable sine waves. While patients showed large phase lags that increased with frequency in
620 both conditions, controls only showed large phase lags in the sum-of-sines condition when the
621 stimulus was unpredictable. We interpret this to mean that the control subjects could predict the
622 movement of the hand *and stimulus* in the single-sine condition, but the cerebellar patients could
623 not.

624 The above results are significant as it has previously been difficult to assess visual
625 feedback control in these patients due to their clear impairments in feedforward control of
626 movement. In Experiment 3, we tested whether patients' intact visual feedback could be
627 exploited to benefit their targeting performance in a reaching task. Indeed, we found that

628 cerebellar patients could leverage their intact, albeit delayed, feedback control ability to improve
629 their movement when we manipulate their visual feedback to assist them.
630

631 ## Delay in Patients but not in Healthy Controls

632 Cerebellar patients are thought to make faulty state estimates of arm motion due to a
633 damaged internal model, which adversely affects their proprioceptive estimates during active
634 movement (N. H. Bhanpuri, Okamura, and Bastian 2013). Thus, we expect them to increase their
635 reliance on visual feedback, which is time delayed compared to proprioceptive feedback. Here
636 we hypothesized that our patients' feedback control system would have an increased delay in
637 comparison to controls. This hypothesis is supported by work that showed that healthy subjects
638 normally rely more on proprioception than vision for feedback control (Crevecoeur, Munoz, and
639 Scott 2016). Based on the Crevecoeur et al. (2016) model, increased variability of the
640 proprioceptive information would lead to increased weighting of visual feedback (Crevecoeur,
641 Munoz, and Scott 2016; Weeks, Therrien, and Bastian 2017).
642

643 Our modeling results reveal that patients have a delay in their feedback loop that
644 approximates what one would expect from visual feedback, while controls appear to have little-
645 to-no feedback delay. One interpretation of the control data is that they are relying on a
646 predictive internal model of their arm dynamics. This would allow them to make corrections
647 even faster than they could using purely proprioceptive feedback. In other words, healthy
648 controls can make corrections for current target movements based on a prediction of the present
649 limb state from outdated measurements and known motor commands, rather than waiting on
650 delayed sensory feedback.

We think that the cerebellar patients' deficits are best explained by their dependence on time-delayed visual feedback, though it is theoretically possible that delays in motor execution could contribute. Previous studies have shown that some patients with cerebellar damage exhibit longer than usual reaction time delays when asked to make discrete, rapid movements (Vilis and Hore 1980; Holmes 1917; Beppu, Suda, and Tanaka 1984; Beppu, Nagaoka, and Tanaka 1987; Day et al. 1998). These reaction time studies aimed to quantify a movement initiation delay as opposed to a feedback delay. Here, we specifically assessed the timing of the in-flight trajectory alterations made while tracking an unpredictable stimulus. While our feedback delay is a type of "reaction time" because this task requires making corrections on the fly, the neural mechanisms underlying these corrections may differ from those responsible for planning and initiation of a rapid movement.

Lastly, while the confluence of data and modeling presented here seems to indicate that patients rely disproportionately on delayed feedback from vision for this tracking task, we cannot rule out the possibility that the control signal may nevertheless include some reliance, albeit weaker, on prediction and proprioception that is not captured by our simplified model.

Modeling Results Support the Cerebellum as a Smith Predictor

Sensorimotor tasks are naturally analyzed using control systems theory and system identification (Roth, Sponberg, and Cowan 2014), and because cerebellar patients' dysmetria resembles a poorly tuned control system, many researchers have analyzed cerebellar behavior using control theory (Luque et al. 2011; Mario Manto 2009; R C Miall et al. 1993; Porrill, Dean, and Anderson 2013).

674

675 Our modeling results indicate that control subjects make corrections based on prediction
676 of a future limb state measurement. While there is some controversy on this (Pelisson et al. 1986;
677 Wolpert, Miall, and Kawato 1998), previous work has proposed that the cerebellum might
678 function in a manner consistent with a Smith Predictor (R C Miall et al. 1993). Essentially, a
679 Smith Predictor is a control architecture that compensates for self-movement feedback delay. To
680 achieve this requires a simulation of the plant in order to predict sensory consequences of motor
681 output, and a simulated delay that "stores" the plant simulation for comparison with delayed
682 feedback. In order to understand the consequences of incorporating a Smith Predictor, consider
683 the generic feedback block diagram of sensorimotor control depicted in Figure 9 (top) and model
684 the brain as either a controller *with* (Figure 9, left) or *without* (Figure 9, right) a Smith Predictor.
685 Surprisingly, upon simplification, we find the exact structures yielded by our modeling results:
686 the patient model matches the simplified block diagram without a Smith Predictor and the age-
687 matched control model matches the simplified block diagram which one. This suggests that an
688 intact cerebellum may be approximated as a Smith Predictor.

689

690 Perhaps the increased feedback delay in the cerebellar patients is unavoidable if one
691 assumes the patients' control systems lack the essential capabilities of a Smith Predictor (making
692 and storing predictive plant simulations). Thus, the apparent increased reliance on visual
693 feedback seen in cerebellar patients may not be a compensatory mechanism at all—perhaps all
694 subjects rely on delayed visual feedback, but healthy subjects disguise the delay using
695 predictions of future measurements of limb state. Patients may simply lack this capability and it
696 is not that they *compensate* for their deficit by relying *more* on visual feedback but instead that

697 the loss of the sensory prediction and storage reveals the visual feedback delay inescapably
698 present in both groups. This would provide some clarity on how cerebellar patients could "learn"
699 to "compensate" in this way even when their cerebellum was damaged.
700
701 At its core, the Smith Predictor has to do with simulating the mechanical plant (and
702 appropriate delay) in order to mitigate the effect of *feedback* delay. But notice that in our model
703 there is a large visuomotor delay on the reference input even with the Smith Predictor in place. In
704 order to compensate for the delayed visual measurement of the stimulus, the brain would need to
705 be able to predict reference motions. To avoid this confound of stimulus prediction, and focus on
706 feedback delay compensation, we fit our models using responses to unpredictable (sum-of-sine)
707 target motions.
708
709 But, what if the target motion were predictable? Previously, it was shown in another
710 species (weakly electric fish) that target predictability can indeed improve tracking performance,
711 and it was hypothesized that this was based on an internal model of predictable reference motion
712 (Roth et al. 2011). Here, we extend this to healthy human subjects who show marked
713 improvement in the single-sine (predictable) tracking task. Cerebellar patients exhibit much more
714 modest improvement in tracking predictable stimuli, suggesting that they may have impairment
715 in both their own plant model predictions and predictions of external sensory references (see
716 Results, Experiment 2). Further data and experiments would be needed to better isolate the
717 effects of cerebellar damage on these potentially disparate functions of the cerebellum.
718

Lastly, even if a healthy cerebellum helps "cancel" expected cursor feedback, this does not imply that visual cursor feedback goes unused: any errors in visual feedback, i.e., cursor self-motion feedback that is not precisely anticipated by the cerebellum, could be highly informative, and recent evidence (Yon et al. 2018) suggests that a predictive model of action–perception could heighten perceptual sensitivity, making self-motion (in this case, cursor) feedback more nuanced and precise.

Potential for Real-World Application

In Experiment 3, we were successfully able to reduce the dysmetria of both the hypermetric and hypometric cerebellar patients in an elbow flexion task. Our visual feedback-control-based intervention was developed based on a control model which represented dysmetria as a mismatch between the patient's internal model of their limb inertia and the actual limb inertia (Nasir H. Bhanpuri, Okamura, and Bastian 2014). Thus, the success of our intervention provides support to this inertial mismatch theory. However, recent evidence based on the application of limb weights suggest that the inertial mismatch theory may be insufficient to explain dysmetria in multi-joint movements (Zimmet, Cowan, and Bastian 2018). Thus, feedback enhancement of multi-joint movements will likely require modifications of the simple acceleration-based controller tested in this paper.

Though our intervention successfully reduces the initial over or undershooting component of the reach, our method does not attempt to correct all aspects of dysmetria. Patients with cerebellar ataxia also typically exhibit increased movement variability. Application of this visual feedback gain does not attempt to reduce the variability of patient reaches. Secondly, our

742 intervention does not completely eliminate the oscillations experienced by the subject after this
743 first correction is made. Moreover, our modeling work does not characterize or explain this
744 increased variability directly. Mild oscillations after the first correction can be seen in Figure 7A.
745 It is possible that adding a damping term to the feedback intervention might be able to address
746 this oscillatory behavior.
747
748 Our results provide an encouraging foundation for future studies because they show that
749 cerebellar patients are capable of using their own intact visual feedback control system to make
750 accurate reaches. Further study is needed to determine whether this intact feedback control
751 system could be leveraged therapeutically to reduce dysmetria without need for a virtual reality
752 system. Alternatively, it is possible that wearable sensory augmentation (for example, tendon
753 vibration or skin stretch) could be used as a surrogate for the vision-based sensory shift provided
754 here. These alternatives are especially important because drug therapy for cerebellar ataxia is not
755 currently viable, leaving rehabilitative and assistive therapies alone as the primary means of
756 treatment for these patients. In any case, we hope that by identifying these intact movement
757 control mechanisms we might help move treatment possibilities forward.
758

ACKNOWLEDGEMENTS

National Institute of Child Health and Human Development HD040289 to AJB

Applied Physics Lab Graduate Fellowship FNACCCX19 to AMZ

James S. McDonnell Foundation Complex Systems Scholar award to NJC

Thanks to James Freudenberg, Brent Gillespie, Matthew Statton, and Sarah Stamper for helpful comments and discussion.

COMPETING INTERESTS

We have no competing financial interests to disclose.

REFERENCES

Adamovich, Sergei V., Mendel B. Berkinblit, Olga Fookson, and Howard Poizner. 1998. "Pointing in 3D Space to Remembered Targets. I. Kinesthetic Versus Visual Target Presentation." *Journal of Neurophysiology* 79 (6): 2833–46.

Bares, Martin, Ovidiu Lungu, Tao Liu, Tobias Waechter, Christopher M Gomez, and James Ashe. 2007. "Impaired Predictive Motor Timing in Patients with Cerebellar Disorders." *Exp Brain Res* 180: 355–65. https://doi.org/10.1007/s00221-007-0857-8.

Beppu, Hirokuni, Masanori Nagaoka, and Reisaku Tanaka. 1987. "Analysis of Cerebellar Motor Disorders By Visually-Guided Elbow Tracking Movement 2. Contribution of the Visual Cues on Slow Ramp Pursuit." *Brain*.

Beppu, Hirokuni, Minami Suda, and Reisaku Tanaka. 1984. "Analysis of Cerebellar Motor Disorders by Visually Guided Elbow Tracking Movement." *Brain* 107: 787–809.

Berens, Philipp. 2009. "CircStat : A MATLAB Toolbox for Circular Statistics." *Journal of Statistical Software* 31 (10). https://doi.org/10.18637/jss.v031.i10.

Bhanpuri, N. H., A. M. Okamura, and A. J. Bastian. 2013. "Predictive Modeling by the Cerebellum Improves Proprioception." *Journal of Neuroscience* 33 (36): 14301–6. https://doi.org/10.1523/JNEUROSCI.0784-13.2013.

Bhanpuri, Nasir H., Allison M. Okamura, and Amy J. Bastian. 2014. "Predicting and Correcting Ataxia Using a Model of Cerebellar Function." *Brain* 137 (7): 1931–44. https://doi.org/10.1093/brain/awu115.

Broersen, Robin, Yoshiyuki Onuki, Abdel R Abdelgabar, Cullen B Owens, Samuel Picard, Jessica Willems, Henk-Jan Boele, Valeria Gazzola, Ysbrand D. Van der Werf, and Chris I De Zeeuw. 2016. "Impaired Spatio-Temporal Predictive Motor Timing Associated with Spinocerebellar Ataxia Type 6." Edited by Warren H Meck. *PLOS ONE* 11 (8). https://doi.org/10.1371/journal.pone.0162042.

Cameron, Brendan D, Cristina de la Malla, and Joan López-Moliner. 2014. "The Role of Differential Delays in Integrating Transient Visual and Proprioceptive Information." *Frontiers in Psychology* 5. https://doi.org/10.3389/fpsyg.2014.00050.

Crevecoeur, X Frédéric, Douglas P Munoz, and Stephen H Scott. 2016. "Dynamic Multisensory Integration : Somatosensory Speed Trumps Visual Accuracy during Feedback Control." *The Journal of Neuroscience : The Official Journal of the Society for Neuroscience* 36 (33): 8598–8611. https://doi.org/10.1523/JNEUROSCI.0184-16.2016.

Day, B. L., P. D. Thompson, a. E. Harding, and C. D. Marsden. 1998. "Influence of Vision on Upper Limb Reaching Movements in Patients with Cerebellar Ataxia." *Brain* 121 (2): 357–72. https://doi.org/10.1093/brain/121.2.357.

Fuentes, Christina T., and Amy J. Bastian. 2010. "Where Is Your Arm? Variations in Proprioception Across Space and Tasks." *Journal of Neurophysiology* 103 (1): 164–71. https://doi.org/10.1152/jn.00494.2009.

Hentschke, Harald, and Maik C. Stüttgen. 2011. "Computation of Measures of Effect Size for

Neuroscience Data Sets." *European Journal of Neuroscience*. https://doi.org/10.1111/j.1460-9568.2011.07902.x.

Holmes, Gordon. 1917. "The Symptoms of Acute Cerebellar Injuries Due to Gunshot Injuries" 40 (4): 461–535. https://doi.org/http://dx.doi.org/10.1093/brain/40.4.461.

Luque, Niceto Rafael, Jesús Alberto Garrido, Richard Rafael Carrillo, Olivier J M D Coenen, and Eduardo Ros. 2011. "Cerebellarlike Corrective Model Inference Engine for Manipulation Tasks." *IEEE Transactions on Systems, Man, and Cybernetics, Part B: Cybernetics* 41 (5): 1299–1312. https://doi.org/10.1109/TSMCB.2011.2138693.

Madhav, Manu S, Sarah a Stamper, Eric S Fortune, and Noah J Cowan. 2013. "Closed-Loop Stabilization of the Jamming Avoidance Response Reveals Its Locally Unstable and Globally Nonlinear Dynamics." *The Journal of Experimental Biology* 216 (22): 4272–84. https://doi.org/10.1242/jeb.088922.

Manto, M., E. Godaux, and J. Jacquy. 1994. "Cerebellar Hypermetria Is Larger When the Inertial Load Is Artificially Increased." *Annals of Neurology* 35 (1): 45–52. https://doi.org/10.1002/ana.410350108.

Manto, Mario. 2009. "Mechanisms of Human Cerebellar Dysmetria: Experimental Evidence and Current Conceptual Bases." *Journal of Neuroengineering and Rehabilitation* 6. https://doi.org/10.1186/1743-0003-6-10.

McRuer, Duane T., and Ezra S. Krendel. 1974. "Mathematical Models of Human Pilot Behavior." Paris.

Miall, R. Chris, Lars O. D. Christensen, Owen Cain, James Stanley, and JC Rothwell. 2007. "Disruption of State Estimation in the Human Lateral Cerebellum." *PLoS Biology* 5 (11): 2733–44. https://doi.org/10.1371/journal.pbio.0050316.

Miall, R C, D J Weir, Daniel M. Wolpert, and J F Stein. 1993. "Is the Cerebellum a Smith Predictor?" *Journal of Motor Behavior* 25 (3): 203–16. https://doi.org/10.1080/00222895.1993.9942050.

Morton, Susanne M, and Amy J Bastian. 2006. "Cerebellar Contributions to Locomotor Adaptations during Splitbelt Treadmill Walking." *Journal of Neuroscience* 26 (36): 9107–16. https://doi.org/10.1523/JNEUROSCI.2622-06.2006.

Mostafavi, Sayyed Mostafa, Parvin Mousavi, Sean P Dukelow, and Stephen H Scott. 2015. "Robot-Based Assessment of Motor and Proprioceptive Function Identifies Biomarkers for Prediction of Functional Independence Measures." *Journal of Neuroengineering and Rehabilitation* 12 (1): 105. https://doi.org/10.1186/s12984-015-0104-7.

Paillard, J., and M. Brouchon. 1974. "A Proprioceptive Contribution to the Spatial Encoding of Position Cues for Ballistic Movements." *Brain Research* 71 (2–3): 273–84. https://doi.org/10.1016/0006-8993(74)90971-8.

Pelisson, D., C. Prablanc, M.A. A Goodale, and M. Jeannerod. 1986. "Visual Control of Reaching Movements without Vision of the Limb II. Evidence of Fast Unconscious Process Correcting the Trajectory of the Hand to the Final Position of a Double-Step Stimulus." *Exp Brain Res* 62 (2): 303–11. https://doi.org/10.1007/BF00238849.

Porrill, John, Paul Dean, and Sean R. Anderson. 2013. "Adaptive Filters and Internal Models: Multilevel Description of Cerebellar Function." *Neural Networks* 47: 134–49. https://doi.org/10.1016/j.neunet.2012.12.005.

Roth, E., S. Sponberg, and N. J. Cowan. 2014. "A Comparative Approach to Closed-Loop Computation." *Current Opinion in Neurobiology* 25: 54–62. https://doi.org/10.1016/j.conb.2013.11.005.

Roth, E., K. Zhuang, S. A. Stamper, E. S. Fortune, and N. J. Cowan. 2011. "Stimulus Predictability Mediates a Switch in Locomotor Smooth Pursuit Performance for Eigenmannia Virescens." *The Journal of Experimental Biology* 214 (Pt 7): 1170–80. https://doi.org/10.1242/jeb.048124.

Smith, Maurice A, and Reza Shadmehr. 2005. "Intact Ability to Learn Internal Models of Arm Dynamics in Huntington's Disease But Not Cerebellar Degeneration." *Journal of Neurophysiology* 93: 2809–21. https://doi.org/10.1152/jn.00943.2004.

Smith, Maurice, Jason Brandt, and Reza Shadmehr. 2000. "Motor Disorder in Huntington's Disease Begins as a Dysfunction in Error Feedback Control." *Nature* 403 (6769): 544–49. https://doi.org/10.1038/35000576.

Taylor, M M, and C Douglas Creelman. 1967. "PEST: Efficient Estimates on Probability Functions." *The Journal of the Acoustical Society of America* 41 (4): 782–87. https://doi.org/10.1121/1.1910407.

Trouillas, P., T. Takayanagi, M. Hallett, R. D. Currier, S. H. Subramony, K. Wessel, A. Bryer, et al. 1997. "International Cooperative Ataxia Rating Scale for Pharmacological Assessment of the Cerebellar Syndrome." *Journal of the Neurological Sciences* 145 (2): 205–11. https://doi.org/10.1016/S0022-510X(96)00231-6.

Vilis, T., and J. Hore. 1980. "Central Neural Mechanisms Contributing to Cerebellar Tremor Produced by Limb Perturbations." *Journal of Neurophysiology* 43 (2): 279–91.

Weeks, Heidi M., Amanda S. Therrien, and Amy J. Bastian. 2017. "Proprioceptive Localization Deficits in People with Cerebellar Damage." *Cerebellum* 16: 427–37. https://doi.org/10.1007/s12311-016-0819-4.

Wolpert, Daniel M, R.Chris Miall, and Mitsuo Kawato. 1998. "Internal Models in the Cerebellum." *Trends in Cognitive Sciences* 2 (9): 338–47. https://doi.org/10.1016/S1364-6613(98)01221-2.

Yon, Daniel, Sam J. Gilbert, Floris P. de Lange, and Clare Press. 2018. "Action Sharpens Sensory Representations of Expected Outcomes." *Nature Communications*. https://doi.org/10.1038/s41467-018-06752-7.

Zimmet, Amanda M., Noah J. Cowan, and Amy J. Bastian. 2018. "Patients with Cerebellar Ataxia Do Not Benefit from Limb Weights." *The Cerebellum*, August. https://doi.org/10.1007/s12311-018-0962-1.

CODE/DATA REPOSITORY

The dataset and code used in this paper will be uploaded to Dataverse and made publicly available.

FIGURES

Figure 1 – Experimental Setup

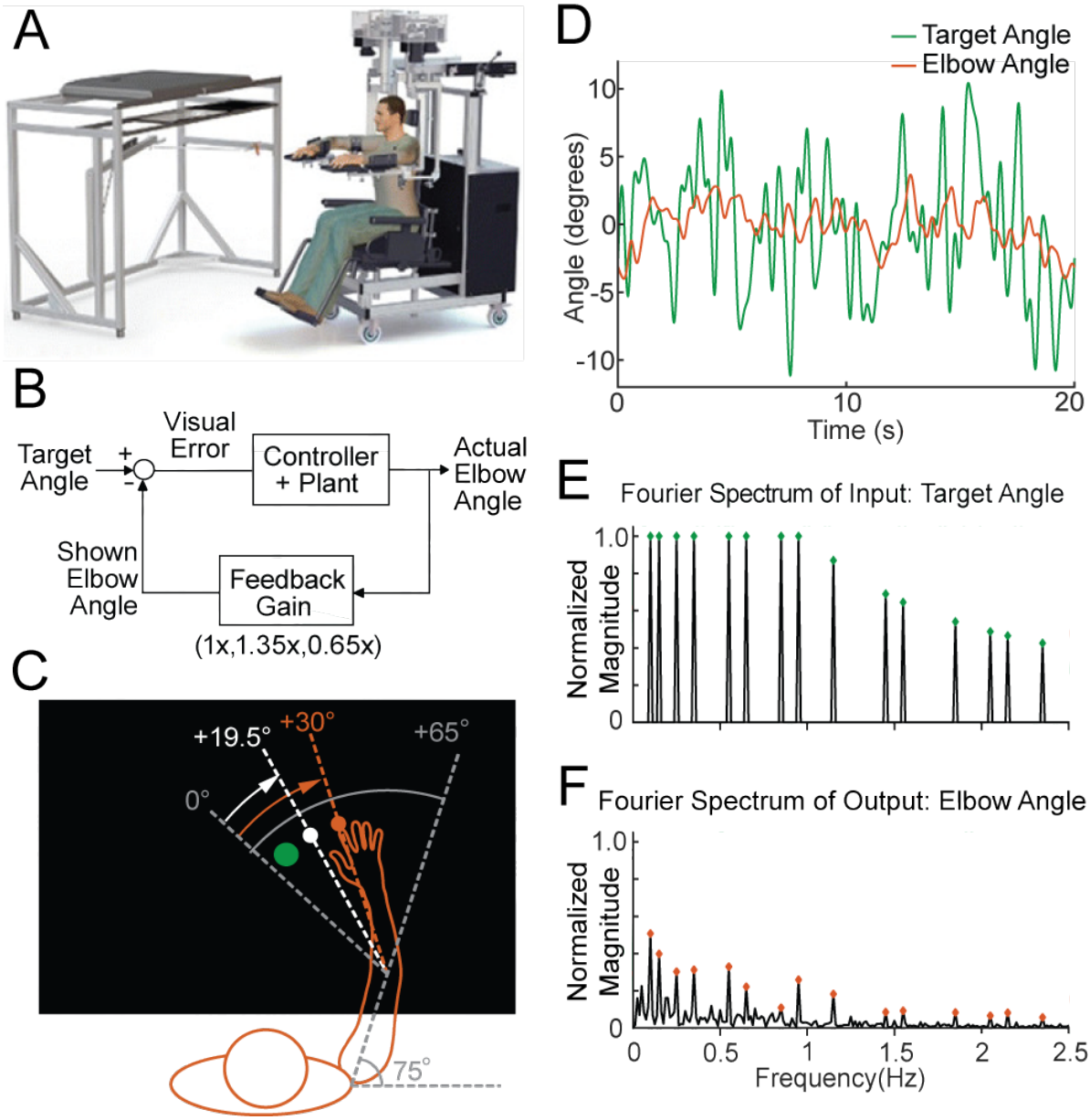

Figure 1 *The experimental paradigm*. **A** The Kinarm Exoskeleton robot system (BKIN Technologies Ltd.) where all tasks are executed. Image is taken from (Mostafavi et al. 2015). **B** This block diagram shows our experimental paradigm for experiment 1. The actual elbow angle (orange in C) is multiplied by a feedback gain to compute the shown elbow angle (white dot in C). **C** A schematic view of the Kinarm screen in the 0.65 Feedback Gain condition. The subject's shoulder is locked at a 75° angle. The green dot is the target dot. The green dot oscillates according to the sum-of-sines pattern along an arc with a radius equivalent to the forearm + hand + finger length. The sum-of-sines pattern is centered about the 0° angle. This 0° centerline is at a 65° angle from the subject's straight arm position. The subject could not see their fingertip (orange dot) or arm position. The angle of the white dot (visible to the subject) is equal to 0.65 times the actual fingertip angle in orange (0.65 · 30° = 19.5°). **D** Sample data (20 s) for a single cerebellar patient showing the angles traversed by the target dot during the sum-of-sines task (green) and by the fingertip (orange, averaged over 5 trials). **E** The normalized Fourier spectrum of the input sum-of-sines signal (green trace in D). **F** The spectrum of the response by a single cerebellar patient over five trials (orange trace in D).

Figure 2 – Interpreting Phasor Plots

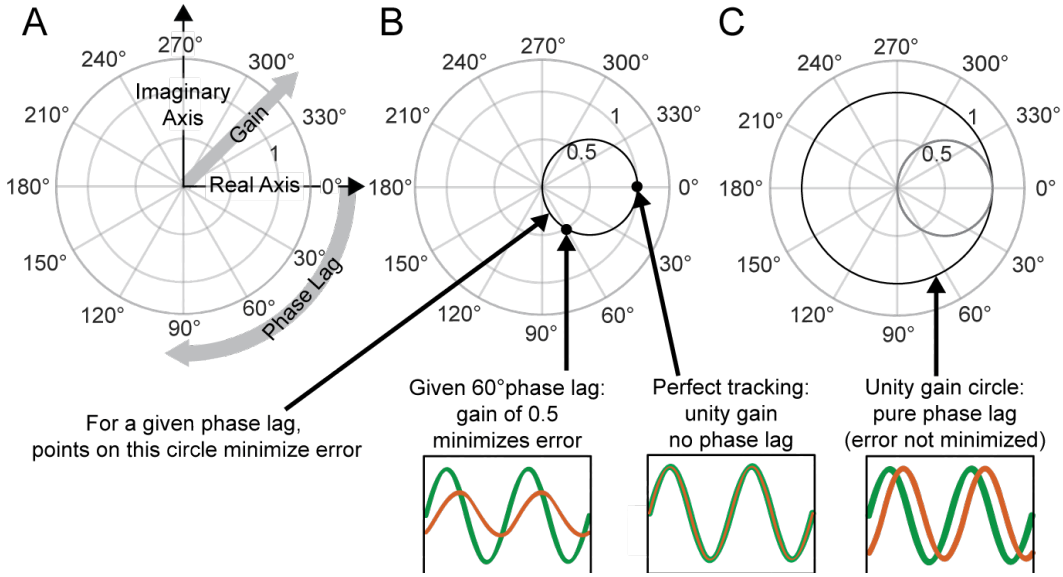

Figure 2 *Interpreting Phasor Plots*. **A-C** Brief explanation of phasor plots, which are explained in depth in Methods in "Phasor Plot." **A** Illustration of the relationship between the real and imaginary components of the complex numbers and the gain and phase lag. **B** The bold black circle illustrates the gains that minimize error given a particular phase lag (veridical feedback condition only). **C** Points on the bold black circle illustrate a different control strategy than what was asked of our subjects. Points on this circle replicate the input signal without minimizing error between the input and output signals (veridical feedback condition only) due to the phase lag.

Figure 3 – Motion Rescaling under Different Feedback Gains

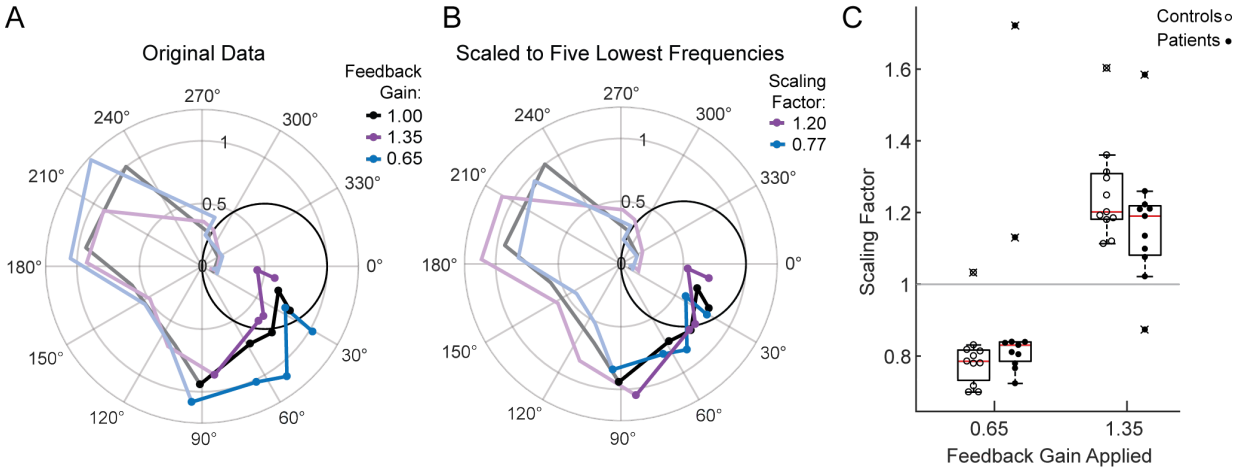

Figure 3 *Motion Rescaling under Different Feedback Gains*. **A** Sample phasor plot data from a single cerebellar patient under all three feedback gain conditions. The dots represent the frequency response at the lowest five frequencies. The solid line traces through the responses at all tested frequencies. The dimmed lines show the frequency responses at the other frequencies tested beyond the five lowest frequencies. **B** Scaled phasor plot data from the same single cerebellar patient. The gain value from D has been multiplied by the scaling factor shown in the legend here to create an overlaid phasor plot. The higher the Scaling Factor, the less effort (in terms of movement magnitude) the subject expended in that condition. Outliers are marked with an x. The outlier subject with the highest Scaling Factor in the 0.65 condition was from the same subject who had the lowest Scaling Factor in the 1.35 condition. **C** Patients and controls respond similarly to the applied Feedback Gain, indicating that they incorporate visual feedback similarly. The higher the Scaling Factor, the less effort (in terms of movement magnitude) the subject expended in that condition. Outliers are marked with an x.

Figure 4 – Modeling

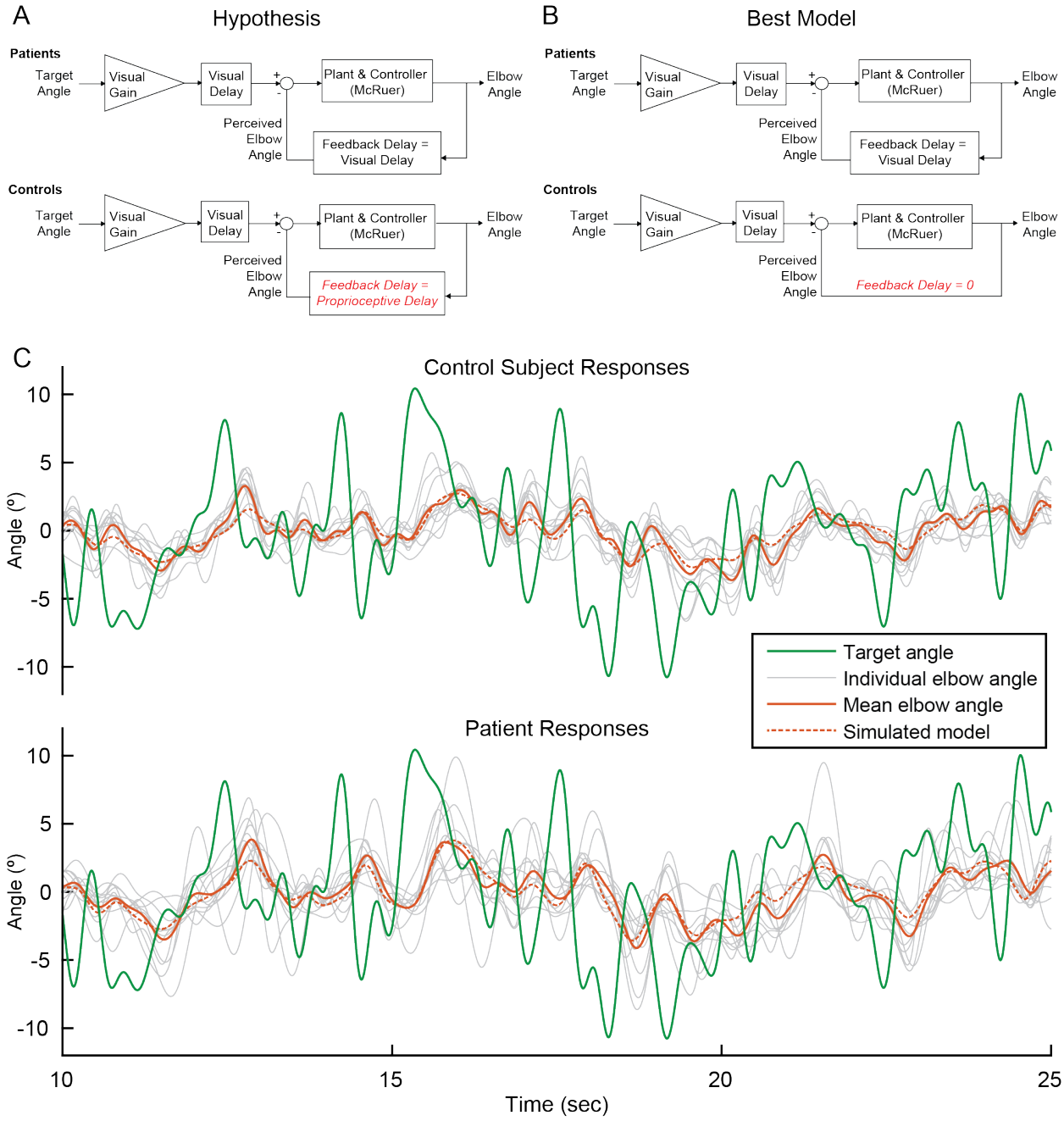

Figure 4 *Modeling.* **A** Our modeling framework was based on the McRuer Crossover model (McRuer and Krendel 1974). This simple model structure lumps the controller and plant as a scaled integrator, and assigns different delays to the measurement of the target from that of self-movement feedback. We hypothesized that the patient and control models would be equivalent except for the magnitude of the feedback delay. The Visual Gain is necessary because, given the complexity and speed of the signal, participants were unable to match the full magnitude of the signal. **B** After our model selection procedure, the Best Model structure was determined to be very similar to our hypothetical model, but with one small difference: the feedback delay for the controls was determined to be zero instead of equivalent to the proprioceptive delay. **C** Time domain visualization of subject and model responses for a typical 15 second time window of our experiments. The same visual target trajectory (green) was played to all patients and controls, and was used in simulation. Individual time-domain elbow-angle responses (light gray) are shown for the 11 control subjects (top plot) and 11 patients (bottom plot). The average subject responses (orange, solid) match with reasonable accuracy the simulated model responses (orange, dashed).

Figure 4 Supplemental 1 – Model Fitting and Model Selection

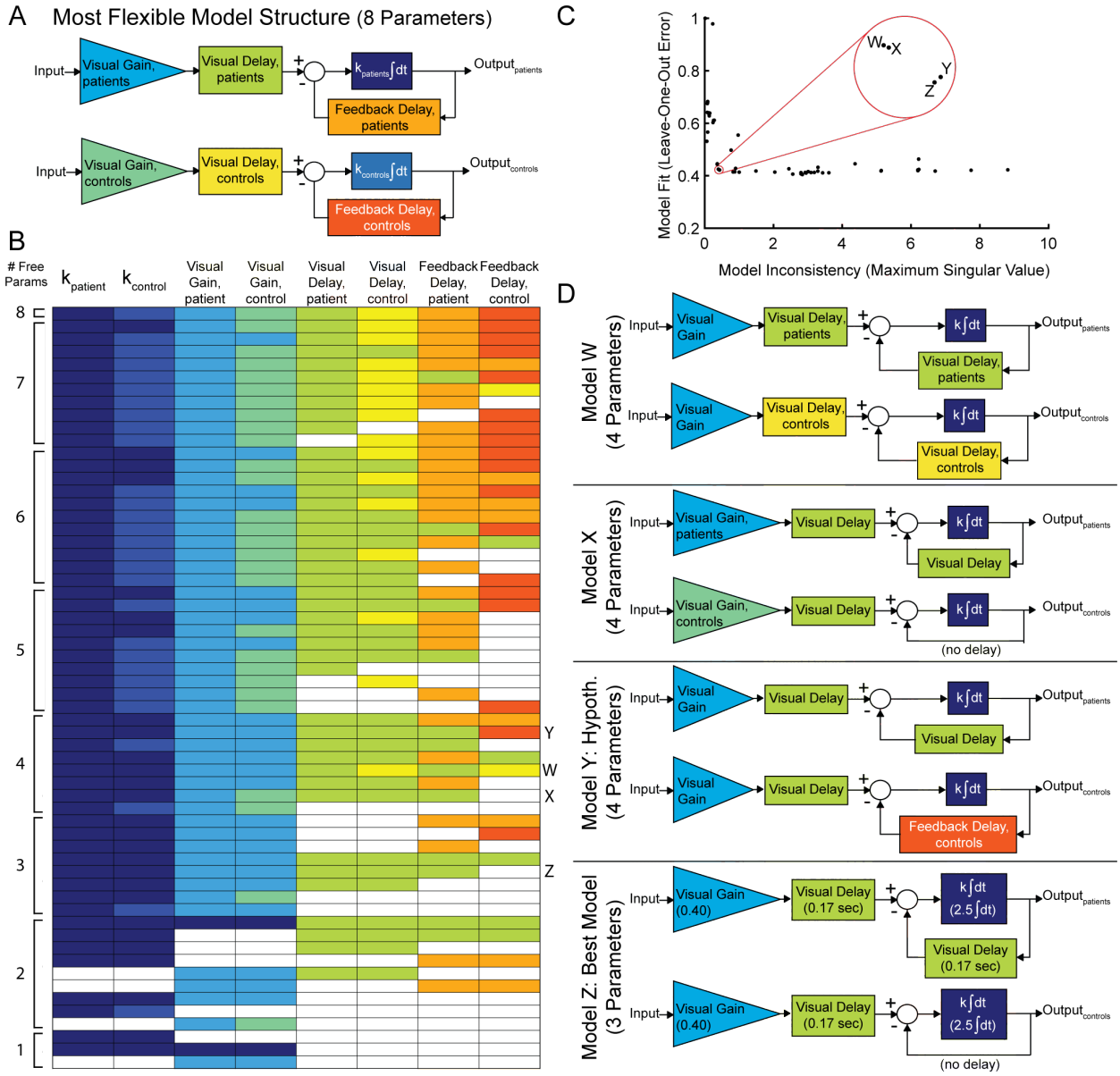

Figure 4S1 *Model Fitting and Model Selection*. We used sum-of-sine data to fit the parameters of a modified McRuer Crossover model (McRuer and Krendel 1974). **A** In the most flexible setting, there are a total of eight free parameters, allowing for patients and controls to have completely independent model parameters. **B** In the model fitting and model selection process, we tested many variations of this model structure. For example, some model structures yoke parameters together or eliminate parameters, and some yoke variables together across patient and control models. This color table specifies all 60 model configurations tested. Each row describes an individual model configuration. Variables with the same color within that row are yoked together for that model configuration. White indicates that the specified variable was removed from the model. The total number of free parameters is shown in the left column. X, Y, and Z in the rightmost column refer to the corresponding top 3 models described in (D). **C** Results of model selection procedure. (Some of the 60 models had model inconsistency values that were orders of magnitude greater than what is shown here, indicating over-parameterization; this figure is truncated to only show the most relevant models). The best four models, highlighted in the red circle, provide the best trade-off between minimizing model inconsistency (i.e., minimizing parameter variability and over-fitting) and minimizing error (improving model fit). The best four models are labeled W, X, Y, and Z. These top four models had nearly equivalent performance according to the model selection criteria. **D** Model W shares the same parameters between patients and controls, except for delay, for which there is a single group-specific parameter for both the feedforward and feedback delay. Model X allows for freedom between

the patient and control models in the visual gain terms. No feedback delay is present in the control subject model. Model Y is our hypothesized model. The cerebellar patient feedback delay is yoked to the visual feedback delay, while the control feedback delay is a free, non-zero parameter. Model Z requires only 3 free parameters and was therefore determined to be our Best Model. No feedback delay is present in the control subject model here as well. The best fit parameter values are shown for this Best Model, Model Z.

Figure 4 Supplemental 2 – Time Domain Validation

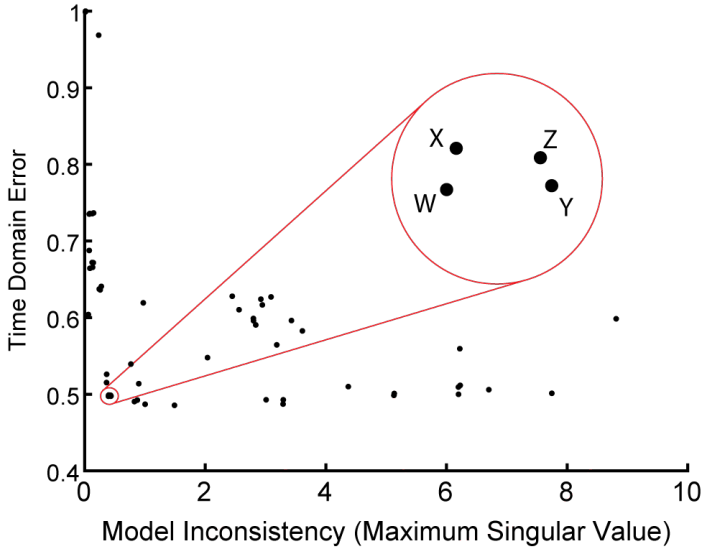

Figure 4S2 *Time Domain Validation*. As in Figure 4S1C, we plotted error versus model inconsistency, but here we used the time-domain error (see Methods). Critically, the time-domain data were not used directly for model fitting, and yet the four top models in the frequency domain are also the four top models in the time domain, validating that our frequency-domain model selection process selected the models that were best in the best time-domain.

Figure 5 –Single-Sine and Sum-of-Sines Phasor Plots

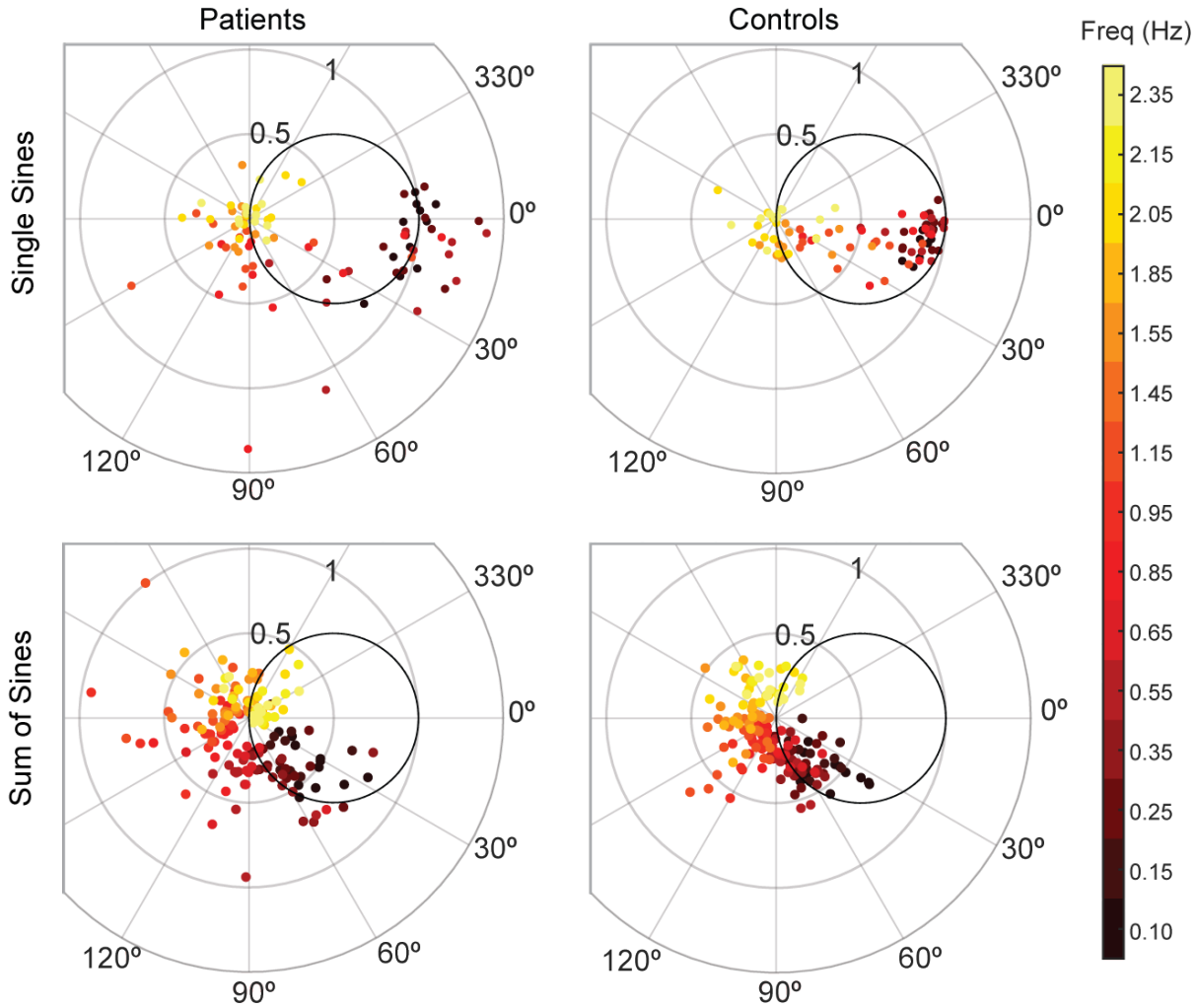

Figure 5 *Patients and controls have categorically different responses to single-sine and sum-of-sine stimuli*. Each data point is the response at a single frequency (magnitude and phase) of a single subject. The patient data in both the single and sum-of-sines conditions are more variable than that of the control subjects. In the single-sines condition, control subjects are able to consistently remain inside the effort/error circle at low frequencies, balancing the tradeoff between effort and error, while patients are not. This result is consistent with previous studies that show patients have impaired prediction.

Figure 6 – Comparison of Phase Lags

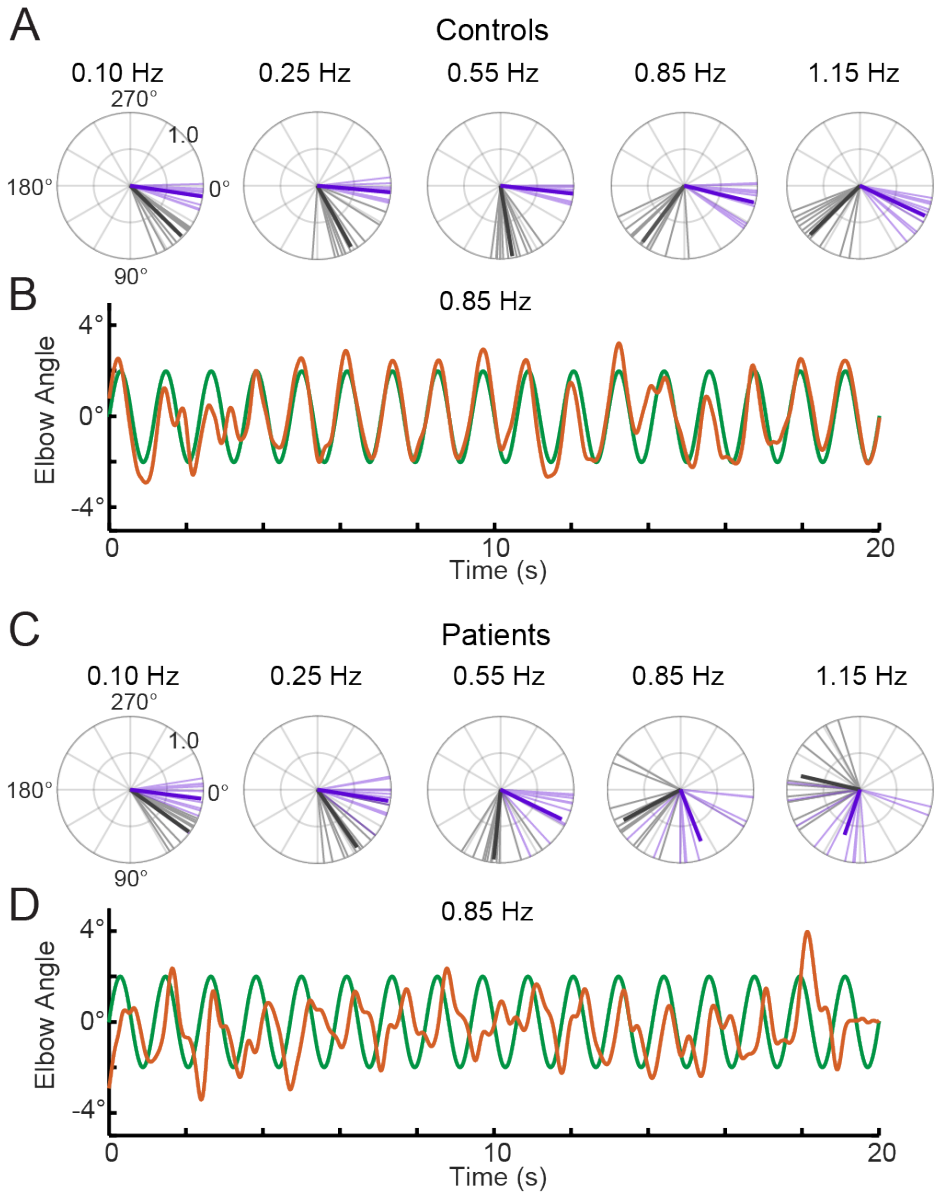

Figure 6 *Phase lags show different patterns between groups.* Polar plot representations showing phase lag for the 5 lowest frequencies common to the single-sine and sum-of-sines conditions. **A.** Control group phase lags. Individual subjects are represented as lighter colored unit vectors and the group mean vector is plotted in bold. Purple indicates the single-sine condition and black represents the sum-of-sines condition. Note that only phase lag is represented on the polar plot (gain is not represented). The Control group is able to track the single-sine stimuli with little or no phase lag, but shows phase lags that increase with frequency in the sum-of-sines condition. **B.** Example response from a control subject tracking a 0.85 Hz single-sine stimuli. The target sine wave is represented in green and the subject performance in orange. Note that this control could predict the single-sine and track it with little or no phase lag. **C.** Cerebellar group phase lags plotted as in A. The Cerebellar patients were able to track the two slowest single-sine stimuli with little phase lag (purple, 0.10 and 0.25 Hz) but then shows increasing phase lags as a function of frequency. Note that 0.10 and 0.25 Hz are extremely slow frequencies that could be followed using only visual feedback control. In the sum-of-sines condition, the cerebellar group shows phase lags that increase with frequency. **D.** Example response from a cerebellar subject tracking a 0.85 Hz single-sine stimuli. In contrast to the control subject, this cerebellar patient shows phase lags relative to the target.

990 ## Figure 7 – Acceleration-Dependent Feedback Reduces Dysmetria

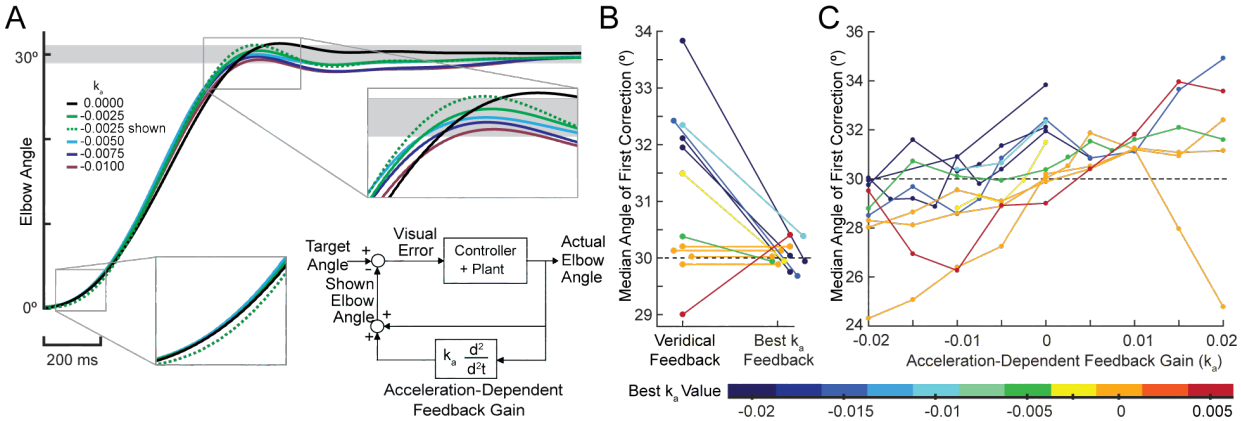

991

992 Figure 7 *Acceleration-dependent feedback reduces dysmetria*. **A** The trajectories from a single cerebellar patient for different
993 Acceleration-Dependent Feedback Gain conditions. The solid lines are average trajectories (across trials for a single subject) at a
994 given Acceleration-Dependent Feedback Gain value. A decrease in the angle of first correction is apparent as the Acceleration-
995 Dependent Feedback Gain decreases. The best Acceleration-Dependent Feedback Gain for this subject was determined to be -
996 0.0025, and the resulting movement trajectory is shown as a solid green line. The dashed green line illustrates the trajectory
997 that is displayed to the subject on the screen for the -0.0025 condition. This example also shows that oscillation around the
998 target remains with Acceleration-Dependent Feedback Gain. The block diagram in the lower right shows how the Acceleration-
999 Dependent Feedback Gain was applied to the visual representation of the fingertip position. **B** The reduction in dysmetria
1000 exhibited by patients when the best Acceleration-Dependent Feedback Gain was applied. Each line represents a single
1001 cerebellar patient. Lines are color coded to indicate the best Acceleration-Dependent Feedback Gain for that subject. **C**
1002 Increasing Acceleration-Dependent Feedback Gain causes increased hypermetria. Again, each line represents a single cerebellar
1003 patient. At the highest gain values, the visual feedback diverged enough from the fingertip position so that some subjects
1004 paused mid-reach, presumably due to the conflicting visual feedback. This yielded the observed drop in median angle of first
1005 correction seen in some subjects in the higher gain conditions. This figure shows only the cerebellar patients. Control subject
1006 data is shown in Figure 8.

Figure 8 – Acceleration-Dependent Feedback: Control Subjects

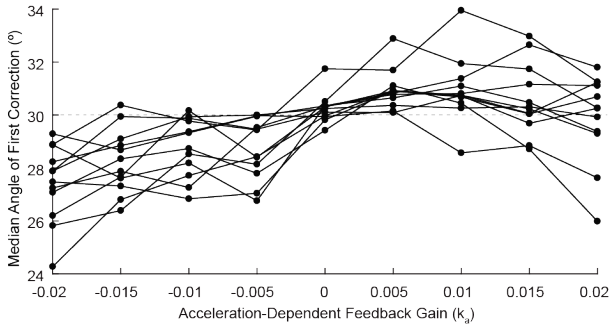

Figure 8 *Acceleration-dependent feedback also affects single reaches in control subjects.* Control subjects' median angle of first correction when completing thirty-degree flexion movements. The expected upward trend in median angle of first correction is visible across subjects. At the largest Acceleration-Dependent Feedback Gains, there is a slight drop off in median angle of first correction. At high gain values, the discrepancy between the cursor and the fingertip became more apparent, causing some subjects to pause mid-reach, resulting in a lower median angle of first correction for these high gain conditions.

Figure 9– Smith Predictor

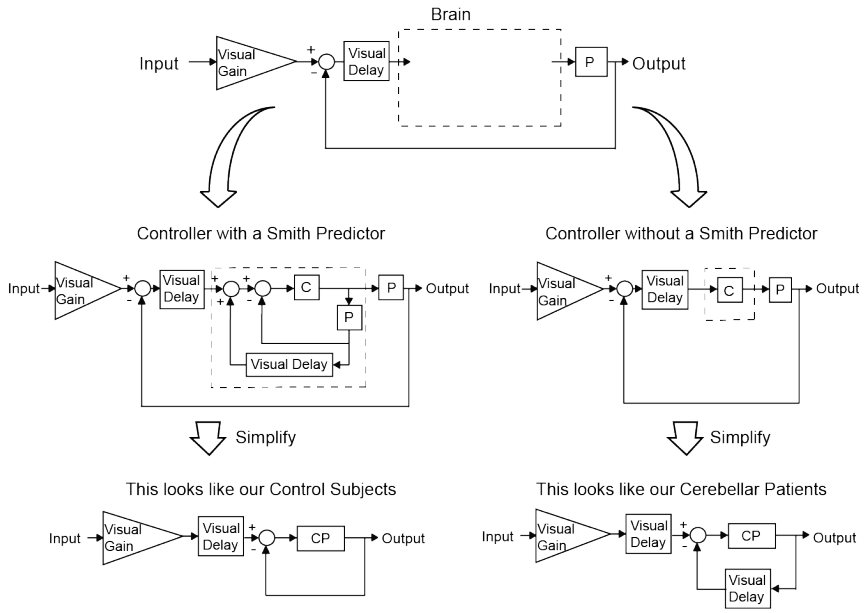

Figure 9 *Our modeling results agree with the theory of the cerebellum as a Smith Predictor*. A basic model for the control system is shown in the top panel. In our experiment, the plant, P, represents the entire mechanical arm system, including the robot exoskeleton arm. A single visual delay block delays the input from both the reference signal and the feedback information. A visual gain scales the amount of the input the subject will attempt to replicate. The brain, illustrated by a dashed box, can be modeled as containing just a controller, C, as shown on the right side. Or, the brain can be modeled as a controller with an accompanying Smith Predictor, as shown on the left side. When these two alternate structures are simplified, we are left with the exact model structures yielded by our previous modeling results.

TABLES

Subject No.	Patient Age	Sex	Pathology	ICARS	Experiments
P1	44	M	SCA8	62	1,2,3
P2	52	M	ADCAIII	28	3
P3	53	M	Sporadic	59	1,2,3
P4	55	F	SCA8	41	3
P5	55	M	OPCA	46	1,2
P6	60	M	MSA-C	63	1,2,3
P7	62	F	Sporadic	36	1,2
P8	62	M	SCA6/8	62	1,2,3
P9	63	M	SCA6	41	3
P10	64	F	SCA6	58	1,2
P11	64	M	ADCAIII	11	1,2,3
P12	65	M	Idiopathic	34	3
P13	66	F	SCA6	41	1,2
P14	67	F	Left Cerebellar Stroke	37	1,2,3
P15	69	F	ADCAIII	52	3
P16	72	F	SCA6	49	3
P17	78	M	Sporadic (Vermis Degen.)	39	1,2

Table 1 The cerebellar patient population that was tested. Not all subjects completed all experiments. Some subjects completed the experiments over two visits.

Model	$k_{patient}$	$k_{control}$	Visual $Gain_{Patients}$	Visual $Gain_{Controls}$	Visual $Delay_{Patients}$ (s)	Visual $Delay_{Controls}$ (s)	Feedback $Delay_{Patients}$ (s)	Feedback $Delay_{Controls}$ (s)
W	2.4	2.4	0.38	0.38	0.18	0.11	0.18	0.11
X	2.6	2.6	0.38	0.41	0.17	0.17	0.17	0
Y	2.5	2.5	0.39	0.39	0.17	0.17	0.17	0.030
Z	2.5	2.5	0.40	0.40	0.17	0.17	0.17	0

Table 2 Model parameters for the four best fit models. Models X, Y, and Z are quantitatively similar; for these models, the McRuer gain (k), visual gain, and visual delay deviated by no more than 5% between patients and controls across all three models, while the feedback gain was consistently equal to the visual delay for the patients, and small (≤30ms) for controls. Model W differs somewhat in model structure and parameters, but also exhibits a smaller feedback delay for controls than patients.

Feedback Gain	k	Visual Gain	Visual Delay (s)	Feedback $Delay_{Patients}$ (s)	Feedback $Delay_{Controls}$ (s)
1.0		<1	Visual Delay	Visual Delay	Proprioceptive Delay
1.35	Decrease	Increase	Unchanged	Unchanged	Unchanged
0.65	Increase	Decrease	Unchanged	Unchanged	Unchanged

Table 3 This is our hypothesis of how we expect the model parameter values indicated in the bottom two rows (1.35 and 0.65 Feedback Gain) will change (with respect to the value obtained in the veridical Feedback Gain condition, Feedback Gain=1.0) with changing Feedback Gains. We expect Visual Delay of approximately 140 to 250 ms, and Proprioceptive Delay approximately 110 to 150 ms (Cameron, de la Malla, and López-Moliner 2014). We also expect Visual Gain to be less than one in the veridical feedback condition because we do not expect the subjects to attempt to replicate the full magnitude of the signal, given that it is a challenging, fast, and unpredictable task.

1037

Feedback Gain	$k_{patient}$	$k_{control}$	Visual $Gain_{Patients}$	Visual $Gain_{Controls}$	Visual $Delay_{Patients}$ (s)	Visual $Delay_{Controls}$ (s)	Feedback $Delay_{Patients}$ (s)	Feedback $Delay_{Controls}$ (s)
1	2.5	2.5	0.40	0.40	0.17	0.17	0.17	0
1.35	2.0	2.0	0.45	0.45	0.17	0.17	0.17	0
0.65	3.3	3.3	0.33	0.33	0.17	0.17	0.17	0

1038 Table 4 The model parameters changed with different applied Feedback Gains in a manner consistent with our prediction.

AUTHOR CONTRIBUTIONS

All three of the authors conceived of the experiments, contributed to the analysis, and participated in the writing. Amanda Zimmet conducted the experiments and collected data.